Science of the Total Environment 752 (2021) 142190

Contents lists available at ScienceDirect

Science of the Total Environment

journal homepage: www.elsevier.com/locate/scitotenv

Lateral carbon fluxes and CO_2 evasion from a subtropical mangrove-seagrass-coral continuum

Anirban Akhand [a,*], Kenta Watanabe [a], Abhra Chanda [b], Tatsuki Tokoro [a,c], Kunal Chakraborty [d], Hirotada Moki [a], Toko Tanaya [a], Jayashree Ghosh [d,e], Tomohiro Kuwae [a]

[a] Coastal and Estuarine Environment Research Group, Port and Airport Research Institute, 3-1-1 Nagase, Yokosuka 239-0826, Japan
[b] School of Oceanographic Studies, Jadavpur University, 188, Raja S. C. Mullick Road, Kolkata 700 032, West Bengal, India
[c] National Institute for Environmental Studies, Center for Global Environmental Research (CGER), Office for Atmospheric and Oceanic Monitoring, 16-2, Onogawa, Tsukuba, Ibaraki 305-8506, Japan
[d] Indian National Center for Ocean Information Services, Ministry of Earth Sciences, Hyderabad 500090, India
[e] School of Ocean Science and Technology, Kerala University of Fisheries and Ocean Studies, Kochi 682506, India

HIGHLIGHTS

- Role of lateral carbon flows in CO_2 dynamics is overlooked in coastal ecosystems.
- Flows and dynamics in a mangrove-seagrass-coral continuum were quantified.
- High-temporal-resolution field observations were used with a mass-balance model.
- Lateral carbon fluxes among the three habitats affected air–water CO_2 fluxes.
- Local and regional lateral carbon flux data can improve carbon budget estimates.

GRAPHICAL ABSTRACT

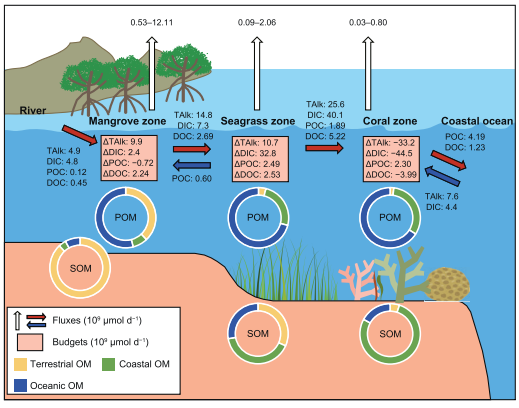

ARTICLE INFO

Article history:
Received 26 June 2020
Received in revised form 19 August 2020
Accepted 2 September 2020
Available online 08 September 2020

Editor: Elena Paoletti

Keywords:
Lateral carbon flux
Air–water CO_2 flux
Mangrove
Seagrass
Coral

ABSTRACT

Mangrove, seagrass, and coral habitats often lie adjacent to each other in the tropics and subtropics. Lateral carbon fluxes and their consecutive effects on CO_2 dynamics and air–water fluxes along the ecosystem continuum are often overlooked. We measured the partial pressure of CO_2 in water and associated biogeochemical parameters with a high temporal resolution and estimated air–water CO_2 fluxes along the ecosystem continuum. Their lateral fluxes were estimated by using a biogeochemical mass-balance model. The results showed that the waters surrounding mangrove, seagrass, and coral habitats acted as a strong, moderate, and weak source of atmospheric CO_2, respectively. The mangrove zone acted as a net source for TAlk, DIC, and DOC, but as a net sink for POC. The contribution of riverine and mangrove-derived OM was substantially high in mangrove sediment, indicating that net transport of POC towards the coastal sea was suppressed by the sediment trapping function of mangroves. The seagrass zone acted as a net source of all carbon forms and TAlk, whereas the coral zone acted as a net sink of TAlk, DIC, and DOC. The lateral transport of carbon from mangroves and rivers offset atmospheric CO_2 uptake in the seagrass zone. DOC degradation might increase DIC, and other biogeochemical processes facilitate the functioning of the coral zone as a DOC sink. However, as a result of DIC uptake by autotrophs, mainly in the coral zone, the whole ecosystem continuum was a net sink of DIC and atmospheric

* Corresponding author at: Port and Airport Research Institute, 3-1-1 Nagase, Yokosuka 239-0826, Kanagawa, Japan.
E-mail addresses: anirban.akhand@gmail.com, akhand@p.mpat.go.jp (A. Akhand).

https://doi.org/10.1016/j.scitotenv.2020.142190

CO_2 evasion was lowered. We conclude that lateral transport of riverine and mangrove-derived DIC, TAlk, and DOC affect CO_2 dynamics and air–water fluxes in seagrass and coral ecosystems. Thus, studies of lateral carbon fluxes at local and regional scales can improve global carbon budget estimates.

1. Introduction

Vegetated coastal ecosystems, such as mangroves, seagrass meadows, and tidal salt marshes, sequester and store substantial amounts of 'blue carbon' in their biomass and underlying sediments (Mcleod et al., 2011; Pendleton et al., 2012; Gulliver et al., 2020; O'Connor et al., 2020; Su et al., 2020). The carbon sequestration function of these ecosystems is recognized to contribute to lowering atmospheric CO_2 concentrations and to the mitigation of global climate change (Brandano et al., 2016; Macreadie et al., 2017; Otani and Endo, 2019; Gnanamoorthy et al., 2020). Coral reefs, found in shallow coastal waters of the tropics and subtropics, also play an important role in the global oceanic carbon cycle (Xu et al., 2019; Roth et al., 2020). Net CO_2 uptake due to organic carbon (OC) production is almost zero (balanced) in coral reef habitats, and net calcification causes reefs to act as a CO_2 source (Lønborg et al., 2019; Watanabe and Nakamura, 2019). Thus, whether coral reefs have a CO_2 sequestration function is still uncertain, and more empirical support is needed to quantify related processes. However, ecosystems dominated by calcifying organisms such as corals contribute to coastal protection because corals build structures that dissipate wave energy (Lovelock and Duarte, 2019; Martins et al., 2019; Langodan et al., 2020). Recently, studies have begun to characterize the functioning and long-term future of these shallow coastal ecosystems (Macreadie et al., 2019).

Mangrove, seagrass, and coral reef ecosystems not only provide ecosystem services to humankind (e.g., climate change mitigation through carbon sequestration); as part of an ecosystem continuum, they also provide services to each other. For example, coral reefs act as breakwaters, creating a low-energy environment for seagrasses and mangroves (Harborne et al., 2006). Mangroves, in turn, provide low light conditions and shade to adjacent corals and prevent their bleaching (Yates et al., 2014; Rogers, 2017). Low pH waters (ongoing ocean acidification) around mangroves help nearby corals to acclimatise to future seawater conditions (Camp et al., 2016). In contrast, seagrass photosynthesis can lead to an increase in the pH and aragonite saturation state of coastal waters (Unsworth et al., 2012).

A substantial part of the carbon assimilated by mangroves is exported to adjacent water bodies by processes such as tidal flushing, pore-water drainage, and litter fall. Tidal export of dissolved inorganic carbon (DIC), dissolved and particulate organic carbon (DOC and POC, respectively) to nearshore seawater accounts for more than 50% of the carbon fixed in the terrestrial compartment of mangroves, out of which a substantial part of DIC is converted to CO_2 and eventually emitted to the atmosphere (Bouillon et al., 2008). However, owing to their export of DIC and alkalinity, mangroves are a long-term atmospheric carbon sink (Maher et al., 2018). Therefore, assessments of the role of mangrove habitats in sequestering carbon and mitigating climate change should include them as a part of the blue carbon paradigm.

Many researchers have investigated the source, fate, and distribution of particulate organic matter (POM) in mangroves and seagrass and exchanges of POM between them (Hemminga et al., 1994; Walton et al., 2014; Chen et al., 2017). In addition, Gillis et al. (2014) reviewed the magnitudes of energy, materials, and organism fluxes at landscape scale in mangrove, seagrass, and coral ecosystems. However, these studies often overlook the water-column carbon sequestration process (i.e., air–water CO_2 exchange) (Kuwae and Hori, 2019). Shallow coastal ecosystems may be autotrophic in nature, but at the same time they can act as a net source of atmospheric CO_2 if they import substantial amounts of organic and inorganic carbon from other ecosystems (Tokoro et al., 2014).

A research gap exists with respect to lateral fluxes of water-column carbon between different shallow vegetated coastal ecosystems and their role in CO_2 dynamics and air–water fluxes. Both mangroves and seagrass meadows can export different carbon forms to the offshore, an ability that enhances the carbon sink potential of these shallow coastal ecosystems (Duarte and Krause-Jensen, 2017; Maher et al., 2018). However, the dynamics of carbon forms in other shallow coastal ecosystems is not well understood. Lateral carbon exchanges of mangrove ecosystems are rarely reported (Maher et al., 2018), and, in particular, little is known about lateral carbon fluxes between mangroves and adjacent seagrass beds and their effects on CO_2 dynamics (Macklin et al., 2019). Direct transfers of carbon between shallow coastal ecosystems are common, but their contributions to carbon stocks at the seascape level remain poorly constrained (Huxham et al., 2018).

We hypothesize that lateral inorganic and organic carbon fluxes from terrestrial and mangrove ecosystems have significant impacts on the CO_2 dynamics and air–water fluxes of adjacent seagrass and coral ecosystems. To test this hypothesis, we used high-temporal-resolution (one minute) data obtained by using various sensors at diurnal scale for direct simultaneous measurement of different biogeochemical parameters, especially the partial pressure of CO_2 in the water [pCO_2 (water)] along a mangrove-seagrass-coral continuum. Use of discrete hourly data might result in the underestimation or overestimation of pCO_2(water) and the air–water CO_2 flux (Rosentreter et al., 2018), whereas use of high-temporal-resolution measurements of pCO_2 (water) and biogeochemical parameters can minimize the data uncertainty. Along with these high-temporal-resolution data, we investigated the spatial distribution of total alkalinity (TAlk) and carbon forms in each ecosystem. The elemental, stable-isotopic, and optical signatures of organic matter (OM) were used to assess the behaviour of OM sources in the water column and sediments.

2. Materials and methods

2.1. Study area

For our study area, we used a site on the coast of Iriomote Island (Japan) as a model of a subtropical environment, where mangrove, seagrass, and coral ecosystems exist along a continuum (Fig. 1). Iriomote Island is situated at a junction between the East China Sea and the north-western Pacific Ocean, and it is also affected by the warm, nutrient-depleted Kuroshio Current. The island has a land surface area of 289 km^2 and a typical subtropical climate, with an annual average air temperature of 24.3 °C and annual precipitation of 2342 mm. Rainfall is especially abundant from May to June (the rainy season) and in August and September (the typhoon season) (Agata, 2006).

2.2. Sample collection and field work

Field surveys were conducted from 3 to 7 August 2017. Temporary platforms were built about 1 km apart for diurnal monitoring of environmental variables of waters in mangrove, seagrass, and coral zones (Figs. 1, S1 and S2, Supplementary material). A pCO_2 analyser and floating sensors were attached to each platform to gather surface-water data (Fig. S1a–e, Supplementary material).

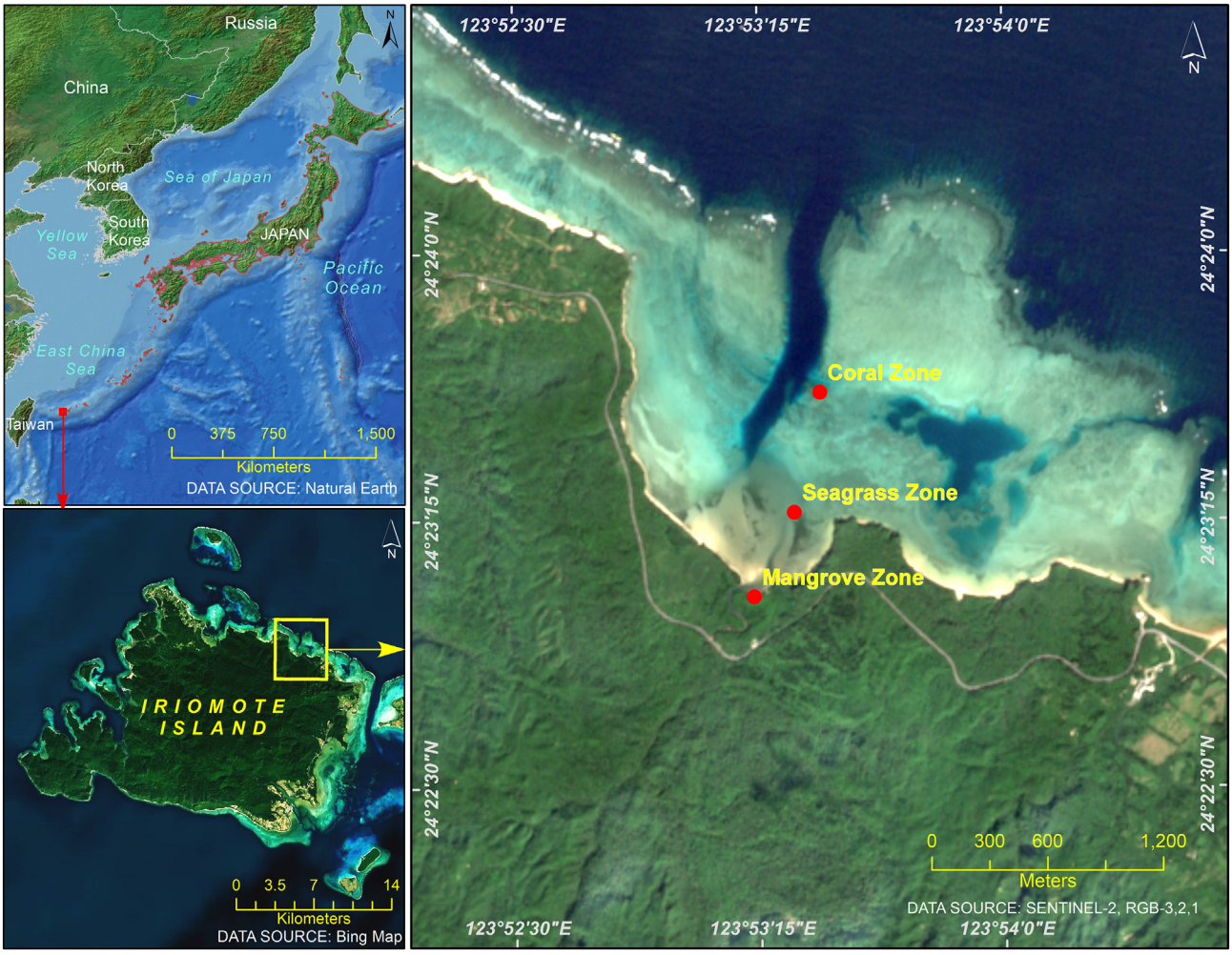

Fig. 1. Location map and sampling sites (red circles) in the mangrove, seagrass, and coral zones of Iriomote Island, Japan. (For interpretation of the references to color in this figure legend, the reader is referred to the web version of this article.)

pCO_2(water) was measured continuously with non-dispersive infrared (NDIR) sensors (CO2-09 and CO2-14, Kimoto Electric, Osaka, Japan) attached to an equilibrator system fitted with a gas permeable membrane (Kayanne et al., 1995; Tokoro et al., 2014). The accuracy and precision of the pCO_2 analyser were ±2 μatm and ±5 μatm (Saito et al., 1995; Kayanne et al., 2005), respectively. We calibrated the analyser using certified CO_2 reference gases (0 μatm and 475 μatm, Taiyo Nippon Sanso Co. Ltd., Tokyo, Japan) in the laboratory before starting the field campaign, and we checked the accuracy on returning to the laboratory after finishing all field work. We found the accuracy to be within ± 2 μatm.

In situ temperature (accuracy and precision ±0.01 °C and ±0.05 °C, respectively) and salinity (accuracy and precision ±0.006 and ±0.03, respectively) were monitored with conductivity-temperature sensors (INFINITY-CT, JFE Advantech, Nishinomiya, Japan). DO (accuracy and precision ±1% and ±1%, respectively) and pH (resolution and precision 0.001 and ±0.003, respectively) were measured with RINKO-I (JFE Advantech) and SP-11 (Kimoto Electric) sensors, respectively. Turbidity (accuracy and precision ±3 FTU) was measured in situ with a fluorometer (COMPACT-CLW, JFE Advantech). Chromophoric dissolved organic matter (CDOM) was measured continuously with an in situ fluorometer (accuracy ±1%, ECO-FL, WET Labs, Philomath, OR, USA). At each site, a submerged depth sensor (INFINITY-WH, JFE Advantech) measured the water depth from the bottom of the water column. An underwater photosynthetically active radiation (PAR) sensor (precision ± 80 μmol m^{-2} s^{-1}, DEFI2-L, JFE Advantech) was also placed at 10 cm above the bottom of the water at each site.

Surface water samples were also collected from each zone (Fig. S1f, Supplementary material) near the platform, as well as from an offshore site, ≈10 km off the coast, used as the seawater end member, and from a site on the Yutsun River, ≈5 km upstream from the mangrove site (salinity 0.19), used as the freshwater end member. Samples were collected from each zone at 3-h intervals during the daytime, starting at about 06:00 (Japan Standard Time). We could not collect water samples during the night-time because of technical difficulties. However, sensor data were collected throughout the diurnal cycle (per minute) at each site, and the morning water samples were collected each day to get the night-time signature insofar as possible. Samples for TAlk and DIC were collected in 250-mL Duran bottles (SCHOTT AG, Mainz, Germany) and poisoned with a saturated solution of mercuric chloride (10 g $HgCl_2$ per 100 mL water; 200 μL per sample bottle) to prevent TAlk and DIC changes due to biological activity (Fig. S1g). Water samples for the DOC and CDOM analyses were filtered through 0.2-μm polytetrafluoroethylene filters (DISMIC–25HP; Advantec, Durham, NC, USA) into precombusted (450 °C for 2 h) 100-mL glass vials and frozen at −20 °C until analysis. Samples for POC, particulate nitrogen (PN), and stable isotope analysis ($\delta^{13}C_{POC}$) were obtained by filtration of 5 to 10 L of water through precombusted (450 °C for 2 h) glass-fibre filters (GF/F, Whatman, Maidstone, Kent, UK), which were stored in the dark at −20 °C until analysis.

Triplicate sediment cores (Fig. S1h–i, Supplementary material) were collected from each zone with an acrylic piston corer. After collection, the cores were immediately preserved by placing them in an ice box; they were transported to the laboratory in the freezer (−15 °C) and then stored in the laboratory at −20 °C until the analyses. The surface sediment layer (0–30 mm depth) in these cores (≈8 cm inner diameter) was used for analyses of total OC (TOC) and total nitrogen (TN) concentrations, and of the stable carbon isotopic signature of sedimentary OC ($\delta^{13}C_{SOC}$).

Mangrove, seagrass, seaweed, microphytobenthos (MPB), and coral samples were collected to determine the elemental and stable isotopic signatures of the OM sources. Leaves and roots of the dominant mangrove species *Rhizophora stylosa*, *Bruguiera gymnorrhiza*, and *Avicennia marina*, and leaves and rhizomes of the dominant seagrass species *Zostera japonica*, *Enhalus acoroides*, *Halodule uninervis*, and *Cymodocea rotundata*, were collected. In addition, parts of the dominant coral species *Heliopora coerulea*, *Porites* spp., and *Acropora* spp., and of two seaweed species, *Digenea simplex* and *Dictiyota* spp., were collected. The MPB was extracted by scraping the surface sediment following the method of Kuwae et al. (2008). All plant and animal samples were stored at −20 °C until analysis.

2.3. Analytical protocol

TAlk and DIC concentrations of surface water samples were measured with a batch-sample analyser (ATT-05; Kimoto Electric) following the Gran plot method (Dickson et al., 2007). A pH meter equipped with a Radiometer Analytical PHC2401-8 Combination Red-Rod pH Electrode (glass body, BNC, Product No. E16M400, Hach, Colorado, USA) was used in these analyses. Three consecutive measurements of certified reference material (Kanso Co. Ltd., Osaka, Japan) were used to determine the accuracy of the TAlk and DIC measurements (3 and 4 μmol kg^{-1} water for TAlk and DIC, respectively).

DOC in each water sample was determined by high-temperature catalytic oxidation with a TOC analyser (TOC-L; Shimadzu, Kyoto, Japan). Potassium hydrogen phthalate (Wako Pure Industries, Osaka, Japan) was used as the standard for this measurement, and the coefficient of variation of the analyses was less than 2%. CDOM absorbance spectra of water samples were recorded from 250 to 700 nm at 1-nm intervals with a UV–visible spectrometer (UV-2450; Shimadzu, Kyoto, Japan) fitted with a 1-cm quartz flow cell and referenced to ultrapure water (Milli-Q water; Millipore, Billerica, MA, USA). The absorbance values at each wavelength (λ) were transformed into absorption coefficients (a_{CDOM}) with Eq. (1):

$$a_{CDOM(\lambda)} = 2.303 \times A_{CDOM(\lambda)}\ (m^{-1}) \quad (1)$$

where A_{CDOM} is the absorbance value. We measured $a_{CDOM(254)}$ as a metric of the aromaticity of the dissolved OM. We calculated specific UV absorbance at 254 nm ($SUVA_{254}$) as follows:

$$SUVA_{254} = A_{CDOM(254)}/[DOC]\ (L\ mg^{-1}\ m^{-1}) \quad (2)$$

where [DOC] is the DOC concentration in mg L^{-1}. Spectral slopes for the 275–295 nm interval ($S_{275–295}$) were calculated by linear regression of the log-transformed a_{CDOM} spectra. Slopes are reported as positive numbers following the mathematical convention for exponential decay. The precision of the CDOM absorption coefficient was 0.005 m^{-1}.

For the chlorophyll-*a* analyses, the GF/F filters were extracted and kept in the dark for 12 h in 90% acetone; then, chlorophyll-*a* concentrations were measured with a UV–visible spectrometer (UV-2450; Shimadzu, Kyoto, Japan) (Lorenzen, 1967).

TOC and TN concentrations and $\delta^{13}C$ were measured with an isotope-ratio mass spectrometer (Delta Plus Advantage, Thermo Electron, Bremen, Germany) coupled with an elemental analyser (Flash EA 1112; Thermo Electron) (analytical precision was ±2% for TOC and TN, and ±0.2‰ for $\delta^{13}C$). Epiphytes and plant debris were carefully removed from seagrass leaves and sediment samples, respectively, before analysis. We analysed one sediment sample from each of the triplicate sediment cores collected from each habitat zone. All samples were oven-dried at 60 °C. Coral tissue was detached from the skeleton with a metal brush after ultrasonication for 30 min. The polyp slurry was oven-dried at 60 °C. The dried samples were acidified with 1 N HCl and dried again at 60 °C to remove inorganic carbon. Vienna PeeDee Belemnite (VPDB) was used as the carbon isotope standard. Based on the standard deviation of internal reference replicates (*L*-histidine [$\delta^{13}C_{VPDB} = -10.19$‰; Shoko Science, Yokohama, Japan]; *L*-alanine [$\delta^{13}C_{VPDB} = -19.6$‰; Shoko Science]), measurement precision was <0.2‰. $\delta^{13}C$ of DIC ($\delta^{13}C_{DIC}$) was also measured with the same isotope-ratio mass spectrometer following the method of Miyajima et al. (1995).

2.4. Estimation of the air–water CO_2 flux

The air–water CO_2 flux (F_{CO2}, μmol CO_2 m^{-2} h^{-1}) was calculated with Eq. (3):

$$F_{CO2} = k \times K_0 \times \Delta pCO_2, \quad (3)$$

where k is the gas transfer velocity (m h^{-1}), K_0 is the solubility coefficient of CO_2 (mol m^{-3} atm^{-1}), and ΔpCO_2 is the difference in CO_2 fugacity (≈partial pressure) between water and air [pCO_2(water) − pCO_2(air)]. In this calculation, we used in situ pCO_2 in air [pCO_2(air)] measured at the study site by pCO_2 analysers. The mole fraction of CO_2 was converted to pCO_2(air) by applying the virial equation of state (Weiss, 1974); as a result, pCO_2(air) was found to be 395 ± 1 μatm. A positive F_{CO2} value denotes a flux from the water to the atmosphere and vice versa. k was calculated by using the observed wind speed and the gas transfer velocity models of Liss and Merlivat (1986), Wanninkhof (1992), and Raymond and Cole (2001), and the best-fit equation of Borges et al. (2004), hereafter referred to as *LM86*, *W92*, *RC01*, and *B04*, respectively. *LM86* was designed to be applicable over a wide range of wind velocities and has been widely used in many studies conducted throughout the world. *W92* is known to be well applicable under steady wind speed conditions, as was the case in this study. However, both *LM86* and *W92* are best suited for deep water and offshore sites. Because this study was carried out in shallow coastal waters, and bottom shear-driven turbulence could not be taken into account, use of *LM86* and *W92* might result in underestimation of the flux. Therefore, to minimize possible flux underestimation and to get a wide range of air–water CO_2 flux data, we also used *RC01* and *B04* to calculate k, because these equations were formulated to estimate estuarine CO_2 fluxes.

The equations used for the calculation of k are as follows:

$$k = 0.17 \times U_{10} \times (660/Sc)^{0.5}. \quad \text{for } U_{10} \leq 3.6\ m\ s^{-1}\ (LM86) \quad (4a)$$

$$k = (2.85 \times U_{10} - 9.65) \times (660/Sc)^{0.5}. \quad \text{for } 3.6 < U_{10} < 13\ m\ s^{-1}\ (LM86) \quad (4b)$$

$$k = 0.31 \times {U_{10}}^2 \times (660/Sc)^{0.5}\ (W92) \quad (5)$$

$$k = 1.91 \times e^{(0.35 \times U10)} \times (660/Sc)^{0.5}\ (RC01) \quad (6)$$

$$k = 5.141 \times {U_{10}}^{0.758} \times (660/Sc)^{0.5}\ (B04) \quad (7)$$

where U_{10} is the wind speed at 10 m above water surface. We used wind speeds measured by the Japan Meteorological Agency meteorological station (Iriomote-Jima) nearest to the study site and corrected for height (Kondo, 2000). *Sc* is the Schmidt number for CO_2 as given by Jähne et al. (1987). K_0 was computed by using the equation given by

Weiss (1974). Of the two *LM86* equations, only Eq. (4a) was used in this study because the mean wind speed was always less than 3.6 m s^{-1} during the study period.

2.5. Estimation of lateral carbon flux

Lateral carbon fluxes (as TAlk, DIC, POC, and DOC) from the riverine freshwater to the coastal ocean through the mangrove, seagrass, and coral zones were estimated by using the Land–Ocean Interactions in the Coastal Zone (LOICZ) biogeochemical box modelling approach. The study area consists of three ecosystems (mangrove, seagrass, and coral), and vertical stratification of salinity within each ecosystem is negligible due to shallow depth. Therefore, the LOICZ biogeochemical model (Gordon et al., 1996) was a reasonable choice for estimating the lateral exchange of various carbon forms among the ecosystems. We constructed three boxes surrounding each zone (Fig. S2, Supplementary material) based on the observed salinity of the freshwater end member, mangrove, seagrass, and coral waters, and the oceanic end member. The areas of the mangrove, seagrass, and coral boxes were 2.24×10^5, 2.48×10^5, and 4.48×10^5 m^2, respectively, and the water depths were 0.43 ± 0.26 m (mean ± SD), 0.80 ± 0.33 m, and 1.12 ± 0.31 m, respectively.

As a first step, the surface area and volume of the three boxes were calculated. Then, the water and salt budgets of the continuum system were computed following Gordon et al. (1996).

The inflows and outflows of water, salt, TAlk, DIC, POC, and DOC were computed with the following equations (De Madron et al., 2003) for each box:

$$(V_q + V_p + V_x) - (V_e + V_x) + V_r = 0 \tag{8}$$

$$(V_x \times S_{ocean}) - (V_x \times S_{sys}) + V_r \times S_r = 0 \tag{9}$$

$$\Delta Y = (V_q \times Y_q + V_x \times Y_{ocean}) - (V_x \times Y_{sys}) + V_r \times Y_r \tag{10}$$

$$V_r = V_e - (V_q + V_p) \tag{11}$$

$$V_x = -V_r \times \frac{S_r}{(S_{ocean} - S_{sys})} \tag{12}$$

where V_q is the volume of river discharge, V_p is the volume of water added by precipitation, V_x is the exchange volume between two boxes, V_r is the residual volume out of the box, V_e is the volume of water evaporated from the surface of the box, S_r is the average salinity of two consecutive boxes, S_{sys} is the salinity of the box the lateral flux of which is being measured, S_{ocean} is the salinity of the next adjacent box towards the sea, Y is the concentration of the constituent of interest (i.e., TAlk, DIC, POC, or DOC), and ΔY is the net imbalance between input and output. Y_{sys} refers to the difference in the concentration of the constituent between two adjacent boxes, Y_q is the riverine concentration of the constituent measured at the freshwater end-member (FWEM) station, Y_{ocean} is the concentration of the constituent at the oceanic end-member station, and Y_r is the average of the concentration of the constituent in the ecosystem box and that at the oceanic end-member station.

The tidal effect on the flux calculation was minimized by averaging all of the data collected during and between high tide and low tide. The uncertainty of the fluxes was calculated as the standard deviation of each constituent. The air–water CO_2 fluxes were not considered in the lateral flux calculations because their effect on the DIC concentration in each box was found to be negligible.

In the study area, the input from sewage was negligible. Rainfall data were obtained from Japan Meteorological Agency (JMA). The groundwater discharge was negligible (0.0000003 m^3 day^{-1}; Mazda and Ikeda, 2006) compared to runoff rate and the precipitation rate, and thus was not considered in this analysis. The amount of rainfall was multiplied by the surface area of the boxes to get the exchange volume among the ecosystems during precipitation. The evaporation dataset (J-OFURO3, newest version V1.1) used for the study area was taken from Tomita et al. (2019). The amount of water lost by evaporation from each individual box was calculated by multiplying the evaporation rate by the surface area of the box. The bathymetry of the study area was obtained from Yamano et al. (2019). The basin area was estimated by using a Digital Topographic Map published by Geospatial Information Authority of Japan. River discharge was estimated by the storage function method (Kimura, 1975; Boyd et al., 1979; Wu et al., 2011) from the basin area and rainfall data.

2.6. Data analysis

To estimate biotic and abiotic changes in the ecosystems, predicted conservative mixing lines were estimated for TAlk, DIC, DOC, POC, PN, and $a_{CDOM(\lambda)}$ by using a linear salinity mixing model. The mixing lines for POC/PN, $SUVA_{254}$, and $S_{275-295}$ were estimated by using the concentrations of the previously mentioned parameters, whereas those for the stable isotope ratios $\delta^{13}C_{POC}$ and $\delta^{13}C_{DIC}$ were based on the formulae proposed by Mook and Tan (1991). For each sample, we calculated the difference between the observed values of DIC and $\delta^{13}C_{DIC}$ and those predicted by conservative mixing (i.e., observed minus predicted) as ΔX, where X represents either DIC or $\delta^{13}C_{DIC}$.

The Bayesian isotopic modelling package, Stable Isotope Analysis in R (SIAR) (Parnell et al., 2010), was used to partition the proportional contributions of potential OM sources to POM and sedimentary OM on the basis of their N/C and $\delta^{13}C$ signatures. We chose to use N/C rather than C/N ratios in the model because the former are statistically more robust; the higher number (the TOC concentration) is the denominator and behaves linearly in the end-member mixtures (Perdue and Koprivnjak, 2007). The contribution from a source with low N/C to sedimentary C_{org} might be overestimated because the N/C ratio generally declines as OM decomposes (Krüger et al., 2015). In contrast, $\delta^{13}C$ changes little during decomposition (Fry, 2006).

The SIAR model works by determining the probability distributions of the sources that contribute to the observed mixed signal while accounting for the uncertainty in the signatures of the sources and for isotopic fractionation. We assumed an isotopic fractionation of 0 and ran the model through 1×10^6 iterations. For each potential source, we report the median and the 95% credible interval (CI) of the estimated proportional contribution of each source.

We defined three potential sources of surface water POM and sedimentary OM to use as end members in the OM mixing model: terrestrial OM (mangrove + riverine POM), coastal OM (seagrass + coral + seaweed + MPB), and oceanic OM. We pooled mangrove and riverine POM by using linear interpolation and a mixing ratio ranging between 0% and 100%. The C/N ratio (13.3) and $\delta^{13}C_{POC}$ (−29.4‰) of riverine POM indicated that it was a mixture of terrigenous sedimentary POM (C/N = 12.17–19.50 mol mol^{-1} and $\delta^{13}C$ = −28.0‰ to −25.4‰; Thornton and McManus, 1994) and POM from terrestrial C3 plants (22.7–50.9 mol mol^{-1} and $\delta^{13}C$ = −29.5‰ to −24.4‰; Kao and Liu, 2000). To suppress divergence of the estimation results, we also pooled seagrass, coral, seaweed, and MPB together. Oceanic OM was defined as the POM collected 10 km offshore.

2.7. Statistical analyses

The significance of the difference in the means of parameters among waters of the mangrove, seagrass, and coral zones was tested by one-way analysis of variance (ANOVA) for normally distributed parameters and the Kruskal Wallis test for non-normally distributed parameters. The normality of all parameters was checked by using the Shapiro-Wilk test. The Pearson correlation coefficient was calculated to assess the relationship between pCO_2(water) and DO (percent saturation). All statistical analyses were carried out with SPSS version 16.0 (SPSS

Inc., Chicago, IL, USA). The results were considered significant at $p < 0.05$.

3. Results

3.1. Biogeochemical variables, carbonate system, and air–water CO_2 flux

The diurnal variability of several parameters showed distinct trends within each complete semidiurnal tidal cycle (Figs. 2 and S3, Supplementary material). The diurnal variability of salinity in particular followed a distinct tidal trend in the mangrove and seagrass zones, with high values during high tide and low values during low tide. In contrast, pCO_2 showed a distinct tidal trend only in mangrove waters, characterized by high values during low tide and low values during high tide.

The mean values of the biogeochemical parameters (water temperature, salinity, and DO) showed significant variability among mangrove, seagrass, and coral zone waters (Table 1). The mean water surface temperature in the zones decreased in the order mangrove, seagrass, and coral ($p < 0.001$), whereas salinity increased from the mangrove to the seagrass zone and then to coral zone ($p < 0.001$). DO increased in the order mangrove, seagrass, and coral ($p < 0.001$). Chlorophyll-*a* concentrations varied between 0.07 and 1.2 mg m^{-3}, and there was no significant difference in the values among the three zones ($p > 0.05$).

Some carbonate chemistry parameters and the air–water CO_2 fluxes were significantly different among mangrove, seagrass, and coral zone waters (Table 1). Mean pH was lowest in the mangrove zone (7.739 ± 0.057) followed by the seagrass (7.920 ± 0.013) and coral zones (8.009 ± 0.177) ($p < 0.001$). Mean pCO_2(water) was highest in the mangrove zone (953 ± 529 μatm) followed by the seagrass zone (483 ± 84 μatm), and it was lowest in the coral zone (415 ± 81 μatm) ($p < 0.001$). The air–water CO_2 flux varied in parallel with the variability of pCO_2(water). pCO_2(water) and DO (percent saturation) were significantly correlated in all three zones (Mangrove, Pearson's r value = −0.61, $p < 0.001$, n = 1907; Seagrass, $r = -0.69$, $p < 0.001$, n = 2842; Coral, $r = -0.97$, $p < 0.001$, n = 2995) (Fig. S4, Supplementary material).

Other carbonate chemistry parameters (TAlk and DIC) did not show any statistically significant differences among waters from the three zones ($p > 0.05$, Table 1). Most TAlk and DIC values in the mangrove and seagrass zones plotted above the conservative mixing line whereas those in the coral zone plotted along or below the line (Fig. 3a and b). Most $\delta^{13}C_{DIC}$ values plotted below the conservative mixing line (Fig. 3h). For the most part, positive ΔDIC values were associated with

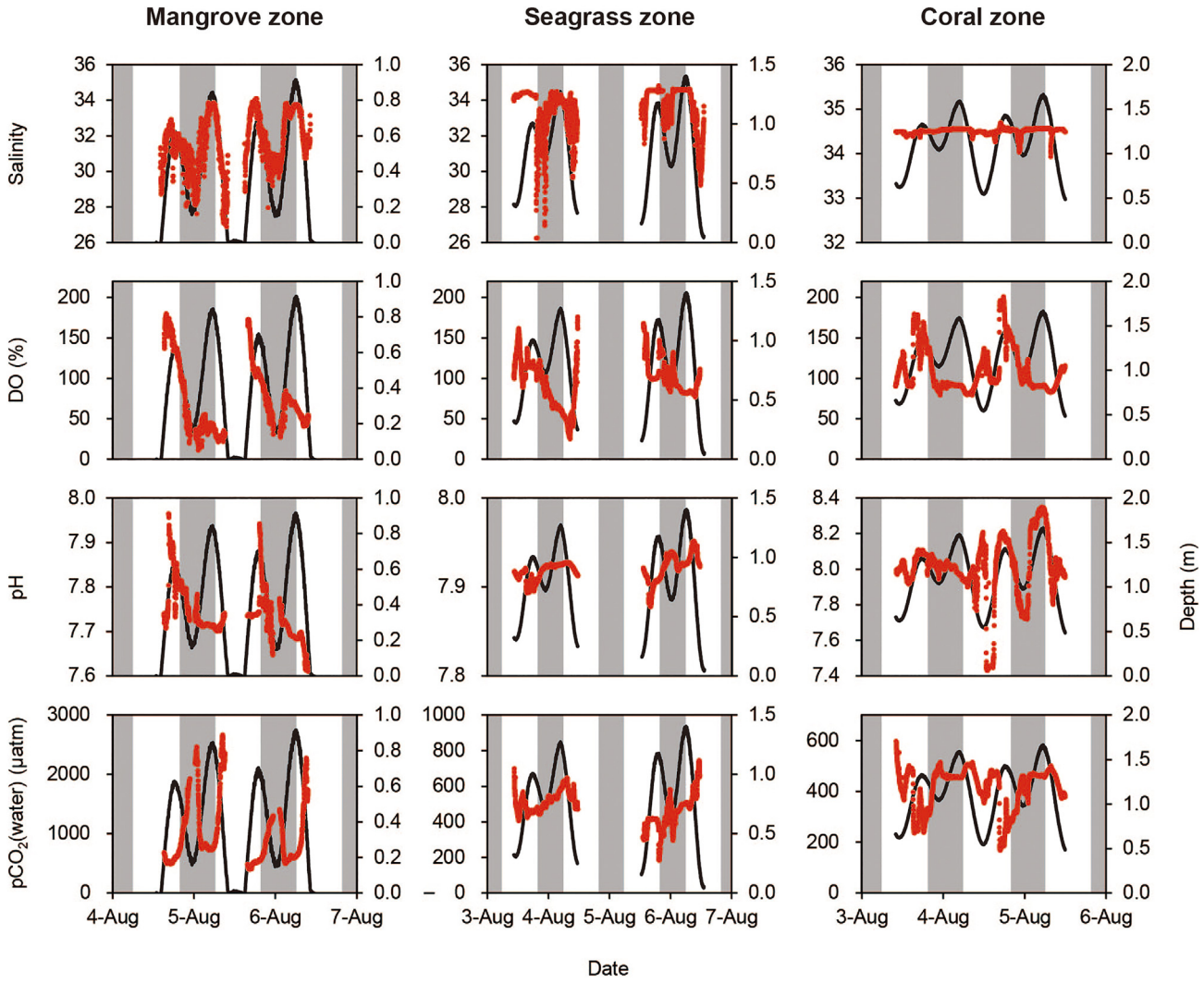

Fig. 2. Temporal (diurnal) variability of salinity, dissolved oxygen (DO), pH, pCO_2(water) and the air–water CO_2 flux in the mangrove, seagrass, and coral zones. Tidal height is represented by water depth. The red lines represent the parameters indicated on the left vertical axis, and the black lines represent water depth (right axis). The grey bands represent the night-time portion of the diurnal cycle. The data were collected from 3 August to 7 August 2017. (For interpretation of the references to color in this figure legend, the reader is referred to the web version of this article.)

Table 1
Mean values (±standard deviation) and ranges of all physico-chemical, carbonate chemistry, and organic-matter parameters measured in mangrove-, seagrass-, and coral-adjacent waters. The statistical significance of differences among the three zones was tested by one-way ANOVA or the Kruskal-Wallis test.

Parameter	Mangrove water	Seagrass water	Coral water	*p* value
Water temperature (°C)	31.86 ± 2.42 (28.40–39.70) n = 2349	31.14 ± 1.66 (28.66–35.81) n = 2980	30.64 ± 1.37 (28.90–35.18) n = 2994	$p < 0.001$
Salinity	31.68 ± 1.53 (26.89–34.09) n = 2349	33.61 ± 1.27 (26.24–34.81) n = 2980	34.51 ± 0.07 (33.93–34.70) n = 2994	$p < 0.001$
Dissolved oxygen (mg L^{-1})	5.49 ± 2.83 (0.82–12.03) n = 1907	7.04 ± 1.84 (1.89–12.33) n = 2842	8.13 ± 1.82 (6.00–14.13) n = 2995	$p < 0.001$
Dissolved oxygen (% saturation)	76.24 ± 42.53 (11.25–180.00) n = 1907	95.45 ± 26.82 (25.16–175.94) n = 2842	109.47 ± 27.37 (79.23–201.15) n = 2995	$p < 0.001$
Chlorophyll-*a* (mg m^{-3})	0.28 ± 0.09 (0.19–0.37) n = 3	0.52 ± 0.34 (0.30–1.20) n = 6	0.26 ± 0.18 (0.07–0.65) n = 10	$p > 0.05$
pH	7.739 ± 0.057 (7.610–7.965) n = 1946	7.920 ± 0.013 (7.878–7.952) n = 2832	8.009 ± 0.177 (7.431–8.348) n = 2985	$p < 0.001$
Total alkalinity (μmol kg^{-1})	2291 ± 390 (1768–3053) n = 7	2219 ± 45 (2149–2260) n = 10	2211 ± 44 (2110–2251) n = 10	$p > 0.05$
Dissolved inorganic carbon (μmol kg^{-1})	2074 ± 408 (1738–2883) n = 7	1933 ± 59 (1798–2044) n = 10	1878 ± 103 (1638–1957) n = 10	$p > 0.05$
pCO_2(water) (μatm)	953 ± 529 (401–2667) n = 1939	483 ± 84 (183–745) n = 2832	415 ± 81 (168–597) n = 2972	$p < 0.001$
Dissolved organic carbon (μM)	104.0 ± 19.6 (70.2–133.6) n = 7	79.6 ± 16.6 (40.9–97.9) n = 10	67.7 ± 11.0 (45.3–84.8) n = 10	$p < 0.001$
Particulate organic carbon (μM)	63.5 ± 110.2 (13.6–313.0) n = 7	12.1 ± 4.7 (7.2–21.2) n = 10	7.3 ± 1.4 (5.4–9.8) n = 10	$p < 0.001$
Particulate nitrogen (μM)	5.4 ± 8.7 (1.6–25.1) n = 7	1.3 ± 0.6 (0.8–2.6) n = 10	0.8 ± 0.2 (0.5–1.1) n = 10	$p < 0.001$
$\delta^{13}C_{POC}$ (‰)	−24.4 ± 2.3 (−27.2 to −21.0) n = 7	−20.3 ± 1.7 (−23.2 to −18.1) n = 10	−19.5 ± 1.5 (−21.2 to −16.2) n = 10	$p < 0.001$
$\delta^{13}C_{DIC}$ (‰)	−3.9 ± 2.4 (−6.6 to −0.8) n = 7	−0.7 ± 1.2 (−3.5 to 0.3) n = 10	0.6 ± 0.4 (0.2–1.4) n = 10	$p < 0.001$

negative $\Delta\delta^{13}C_{DIC}$ values, and the few negative ΔDIC were also associated with negative $\Delta\delta^{13}C_{DIC}$ values (Fig. 4).

The complete diurnal and tidal dataset showed that all the three zones in the study area were on average a net source of CO_2 (Table 2). The magnitude of the efflux was highest in the mangrove zone (98–-2253 μmol m^{-2} h^{-1}) followed by the seagrass (15–346 μmol m^{-2} h^{-1}) and coral zones (3–74 μmol m^{-2} h^{-1}) ($p < 0.001$). No negative flux values were observed from the mangrove-surrounding waters (i.e., they never acted as a sink for CO_2) during the diurnal cycle, whereas the seagrass waters acted as a sink during ≈3.5 h of each diurnal cycle (maximum sink magnitude, −183 μmol m^{-2} h^{-1}). Coral waters acted as a sink for CO_2 during ≈8.5 h of the diurnal cycle, and the maximum sink magnitude was also higher in coral waters than in seagrass waters (−206 μmol m^{-2} h^{-1}).

3.2. OM in the water column

OC concentrations and composition varied among waters of the three zones (Table 1). DOC and POC decreased from the mangrove to the seagrass zone and then to the coral zone ($p < 0.001$). DOC concentrations of all mangrove water samples plotted above the predicted conservative mixing line, but some samples of seagrass and coral waters plotted below the conservative mixing line (Fig. 3c). All POC and PN concentrations of mangrove, seagrass, and coral water samples plotted above the predicted conservative mixing line (Fig. 3d and e). Similarly, almost all POC/PN values plotted below the predicted conservative mixing line except for a few water samples from the coral and mangrove zones (Fig. 3f). Almost all $\delta^{13}C_{POC}$ values plotted above the predicted conservative mixing line (Fig. 3g).

Among the three optical signature of CDOM (Fig. 3i–k), $a_{CDOM(254)}$ and $SUVA_{254}$ patterns were similar; they plotted mostly above the conservative mixing line in the mangrove zone, and mostly below the conservative mixing line in the coral zone. In contrast, most $S_{275–295}$ values plotted above the conservative mixing line in the mangrove zone, and below the conservative mixing line in the coral zone, whereas in the seagrass zone, they plotted on both sides of the line. The diurnal variability of CDOM followed a distinct tidal trend, with higher values during low tide and lower values during high tide in all three zones (Fig. S3, Supplementary material).

3.3. OM in surface sediment

Elemental and stable isotopic signatures also showed variability among the three zones (Fig. S5 and Table S1, Supplementary material). Both N/C and $\delta^{13}C_{SOC}$ increased from mangrove to seagrass to coral waters ($p < 0.05$).

3.4. OM source mixing model

The values of $\delta^{13}C$ and C/N could be explained by the mixing of the three potential OM sources (Fig. S5 and Table S2, Supplementary material). The end-member mixing model showed marked differences among the potential sources of POM (Table 3). Oceanic OM was the major component of POM, accounting for 54% (40–65%, 95% credible interval), 71% (62–79%), and 66% (53–75%) of POM in the mangrove, seagrass, and coral zones, respectively. In contrast, terrestrial OM was the major component of sedimentary OM in the mangrove zone at 88% (72–95%), and coastal OM dominated sedimentary OM in the seagrass and coral zones at 41% (25–54%) and 78% (13–94%), respectively.

3.5. Net lateral exchange

The box model results showed that the mangrove zone was a net source of TAlk, DIC, and DOC but a net sink of POC (Fig. 5). The seagrass zone acted as a net source of TAlk and all carbon forms (DIC, DOC, and POC), whereas the coral zone acted as a net sink of TAlk, DIC, and DOC, but a net source of POC (Fig. 5 and Table S3). The mangrove-seagrass-coral continuum acted overall as a net sink of TAlk and DIC; it took up 12.6×10^3 mol day^{-1} of TAlk and 9.3×10^3 mol day^{-1} of DIC. In contrast, the whole continuum exported 4.07×10^3 mol day^{-1} of POC and 0.78×10^3 mol day^{-1} of DOC.

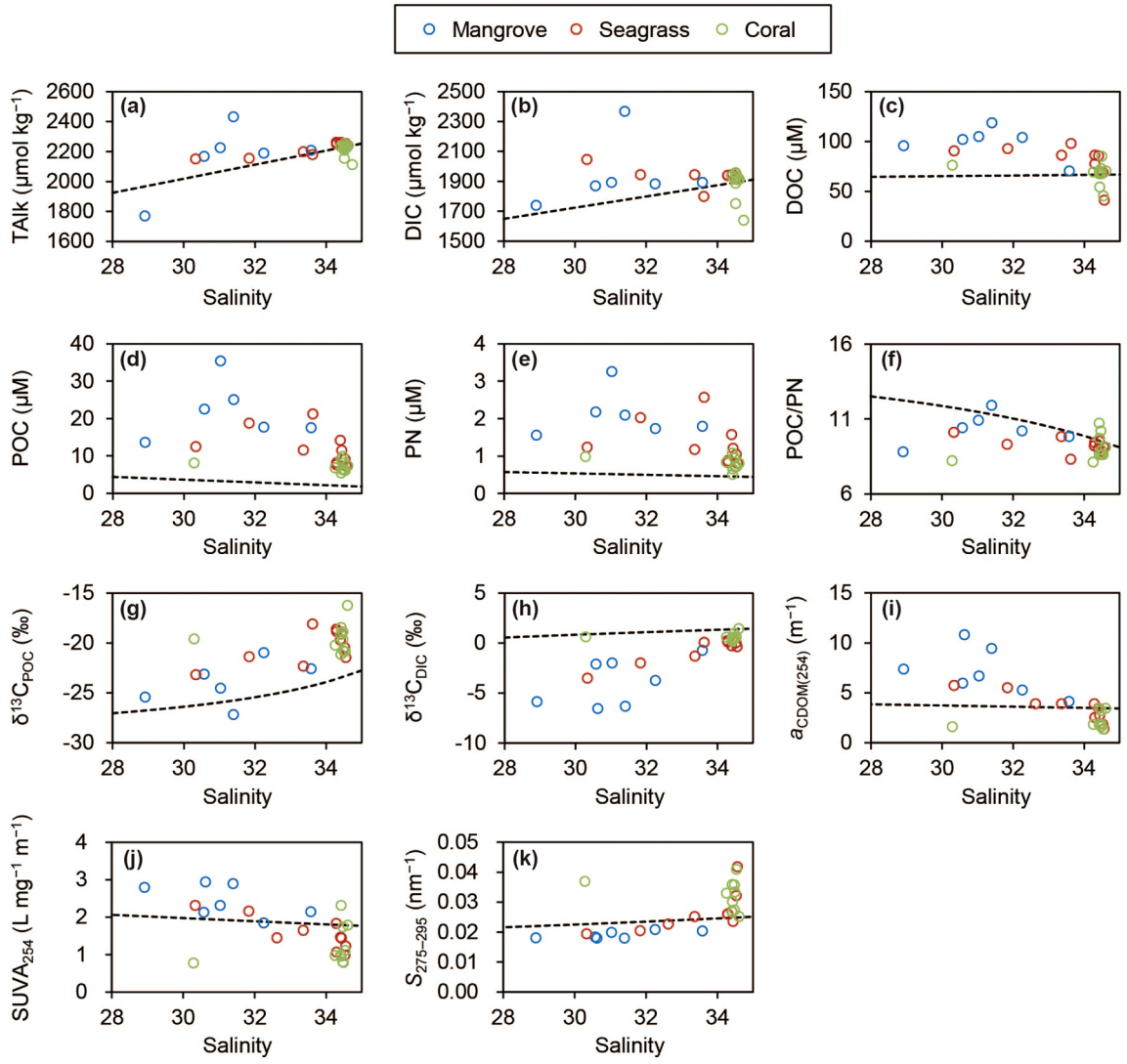

Fig. 3. Distributions of (a) TAlk, (b) DIC, (c) DOC, (d) POC, (e) PN, (f) POC/PN, (g) $\delta^{13}C_{POC}$, (h) $\delta^{13}C_{DIC}$, (i) $a_{CDOM(254)}$, (j) $SUVA_{254}$, and (k) $S_{275-295}$ as a function of salinity in the mangrove, seagrass, and coral zones. The predicted two-end-member conservative mixing distributions of the respective parameters are shown as black dashed lines, based on measured values of the freshwater end member (FWEM) and the oceanic end member (OEM). The FWEM and OEM values for each parameter are shown in Table S4, Supplementary material.

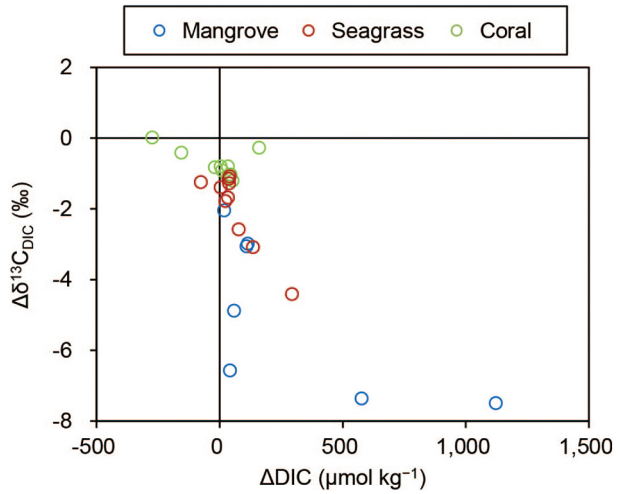

Fig. 4. Deviation plot of ΔDIC vs. $\Delta\delta^{13}C_{DIC}$ in the mangrove, seagrass, and coral zones.

4. Discussion

4.1. The role of the mangrove zone in the continuum system

To the best of our knowledge, this study presents for the first time high-resolution biogeochemical measurements that show the carbon dynamics and air–water CO_2 fluxes in a mangrove-seagrass-coral continuum. Our mass-balance modelling results showed that the mangrove zone acted as a net source of TAlk, DIC, and DOC for the seagrass zone (Fig. 5); this finding supports the hypothesis of Odum and Heald (1975) that carbon and nutrients are 'outwelled' from mangroves in various forms. The POC result in this study, however, does not support the outwelling hypothesis. The two-end-member conservative mixing model for POC (Fig. 3d) suggests that POC is added to the mangrove ecosystem, and the mass-balance model indicates a net lateral POC flux from the seagrass to the mangrove zone (Fig. 5). The relatively low contribution of terrestrial OM to the POM pool in the seagrass zone, compared with its contribution to the mangrove zone, indicate that little mangrove-derived POM reached the seagrass meadow (Table 3). This result might indicate that, as suggested by the mixing model, OM is efficiently trapped in the mangrove sediment rather than retained, as POM, in the water (Table 3). Efficient trapping of riverine suspended

Table 2
Air–water CO_2 fluxes observed in this study (mean ± standard deviation; range in parentheses). *LM86*, *W92*, *RC01*, and *B04* represent gas transfer velocity calculations according to Eq. (4a) (Liss and Merlivat, 1986), Eq. (5) (Wanninkhof, 1992), Eq. (6) (Raymond and Cole, 2001), and Eq. (7) (Borges et al., 2004), respectively.

Air–water CO_2 flux μmol m^{-2} h^{-1}	*LM86*	*W92*	*RC01*	*B04*
Mangrove	98 ± 92 (1–394)	554 ± 522 (6–2227)	1051 ± 991 (12–4225)	2253 ± 2124 (26–9058)
Seagrass	15 ± 15 (−38 to 62)	85 ± 83 (−213 to 348)	161 ± 157 (−404 to 661)	346 ± 337 (−867 to 1416)
Coral	3 ± 14 (−43 to 34)	18 ± 80 (−241 to 194)	34 ± 152 (−457 to 369)	74 ± 325 (−979 to 791)

Table 3
Relative contributions of organic matter (OM) sources estimated by the OM mixing model (using $\delta^{13}C$ and N/C) in particulate OM (POM) and sedimentary OM in the three coastal zones (mangrove, seagrass, and coral zones). The 95% credible interval is shown in parentheses.

OM sources	POM			Sedimentary OM		
	Mangrove	Seagrass	Coral	Mangrove	Seagrass	Coral
Terrestrial OM (mangrove + riverine POM)	38% (28%–48%)	4% (0%–11%)	2% (0%–9%)	88% (72%–95%)	32% (15%–47%)	5% (0%–37%)
Coastal OM (seagrass + coral + seaweed + MPB)	8% (1%–20%)	25% (17%–33%)	32% (22%–41%)	4% (0%–14%)	41% (25%–54%)	78% (13%–94%)
Oceanic OM	54% (40%–65%)	71% (62%–79%)	66% (53%–75%)	8% (0%–22%)	28% (5%–51%)	17% (1%–69%)

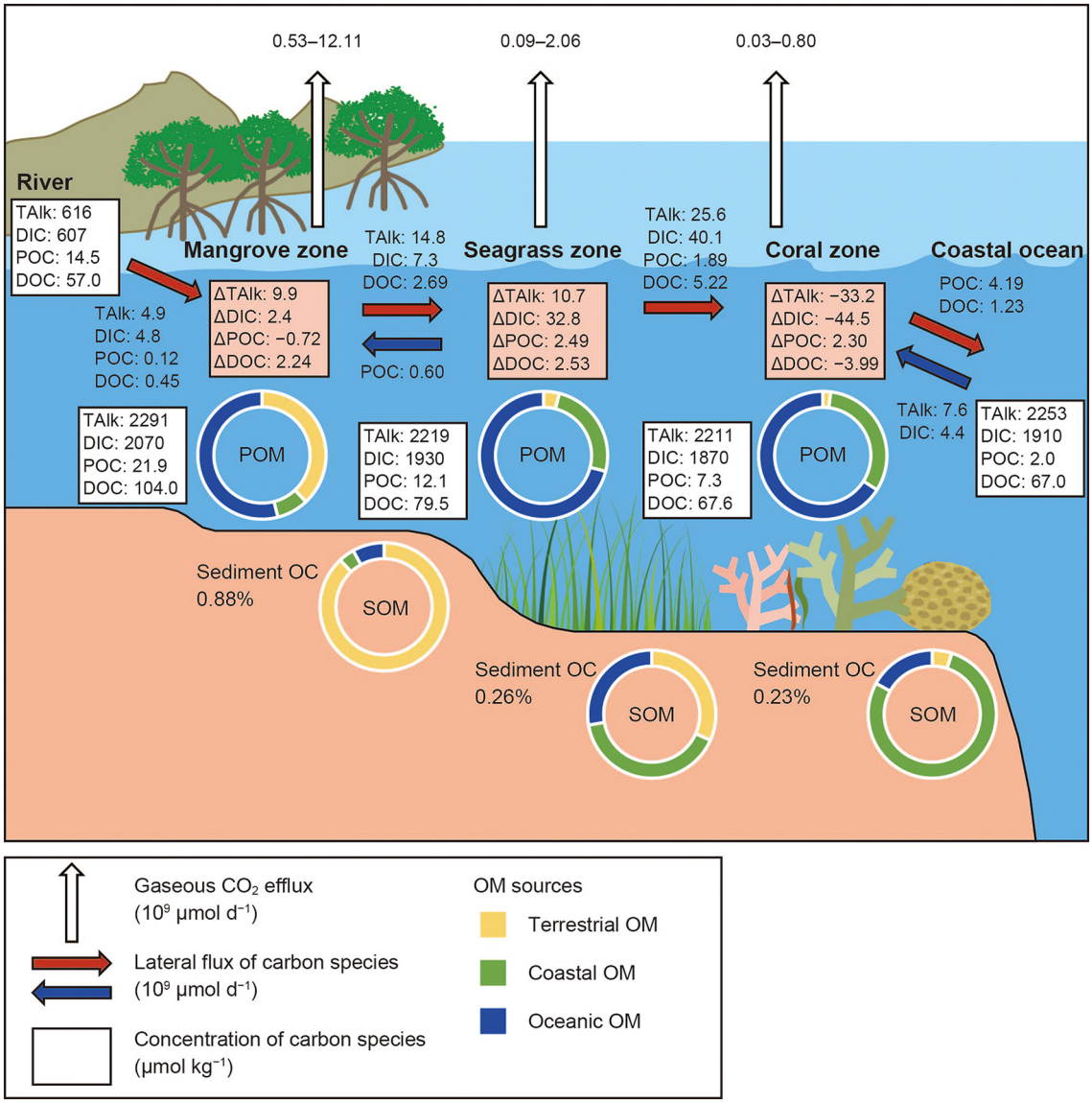

Fig. 5. Schematic diagram of flows of total alkalinity (TAlk) and carbon from riverine freshwater to the coastal ocean through the mangrove, seagrass, and coral zones; area-integrated gaseous CO_2 effluxes from mangrove-, seagrass-, and coral-dominated waters; and sources of POM in water and sediment at the sampling sites. Lateral fluxes of TAlk and carbon forms, dissolved inorganic carbon (DIC), particulate organic carbon (POC), and dissolved organic carbon (DOC), were estimated by using a biogeochemical mass-balance model.

sediment by mangroves, and its mitigation of the sediment load reaching fringing coral reefs, has been reported previously (Victor et al., 2004; Koshiba et al., 2013). Moreover, Victor et al. (2004) reported that trapping of suspended sediment by mangroves is a function of tidal dynamics rather than of the concentration of suspended sediment in river waters. This retention of POM in the mangrove zone has also been attributed to low rainfall (Loneragan et al., 1997) and to minimal river discharge (Ray and Weigt, 2018), both of which would reduce the hydrologic outwelling of POC from mangroves towards the ocean.

Our results show that TAlk was higher than DIC (TAlk:DIC > 1) in the mangrove zone and that more TAlk than DIC was exported from the mangrove zone (Fig. 5). A higher export of TAlk relative to DIC contributes in turn to the lowering of CO_2 evasion from the water (Maher et al., 2018). Previous studies have emphasized that the export of TAlk and DIC from mangroves to coastal seas and eventually to the open ocean (Maher et al., 2013; Sippo et al., 2016; Maher et al., 2018) should be taken into account as a long-term atmospheric carbon sink (Maher et al., 2018).

In the present study, the two-end-member conservative mixing model for CDOM signatures shows that the mangrove zone exported refractory DOC to the offshore. The high values in $a_{CDOM(254)}$ and $SUVA_{254}$ in mangrove waters (Fig. 3i and j) indicate that more refractory and aromatic compounds were exported from the mangrove zone (Tremblay et al., 2007; Bergamaschi et al., 2012). The relatively higher aromaticity of the CDOM observed in the mangrove zone might be due to refractory biopolymers such as lignin, exuded from aquatic vascular plants, and lignin-derived phenols (Watanabe and Kuwae, 2015 and references therein). $S_{275–295}$ (which is generally used as an optical indicator of a potential terrestrial origin of CDOM; Fichot and Benner, 2012) exhibits a gentle slope in mangrove waters, supporting the inference that terrestrial-derived CDOM is added to the mangrove zone.

The mangrove-surrounding waters were supersaturated with respect to atmospheric CO_2 over the entire diurnal cycle (Fig. 2 and Table 2); hence, the mangrove zone acted as a source of CO_2. Mangrove-surrounding waters around the world are sources of CO_2 (e.g., David et al., 2018; Rosentreter et al., 2018; Call et al., 2019; Macklin et al., 2019) because of their substantial organic carbon loading, which is mainly attributed to mangrove biomass, terrestrial detritus, microphytobenthos, and phytoplankton (Borges et al., 2005, 2018; Borges and Abril, 2011; Bouillon and Boschker, 2006). In addition, the efficient exchange and mixing of surface water with pore water through tidal pumping, along with metabolic activity in sediments, leads to increased pCO_2(water) and DIC (Bouillon et al., 2007; Gleeson et al., 2013; Maher et al., 2013; Santos et al., 2012; Sippo et al., 2016). The diurnal variability of pCO_2(water) and the air–water CO_2 flux (Fig. 2) in the present study indicates that tidal pumping in the mangrove zone of pCO_2-rich pore water during ebb tide and pCO_2-poor seawater during flood tide is a major mechanism.

4.2. The role of the seagrass zone in the continuum system

The seagrass zone acted as a source for all carbon forms (DIC, DOC, and POC) and TAlk, despite metabolic consumption processes and deposition in the sediment. Though the combination of positive ΔDIC with negative $\Delta\,\delta^{13}C_{DIC}$ in the deviation plot (Fig. 4) suggests that OM degradation by respiration is the dominant OM mineralisation pathway in the seagrass zone, some positive ΔTAlk deviations (Fig. 3a) are an indicator of TAlk having been added to the seagrass zone, possibly through carbonate dissolution. The role of the seagrass ecosystem as a source of carbon to the adjacent ecosystems and to the coastal sea has been well established (Duarte and Cebrián, 1996; Heck et al., 2008; Duarte and Krause-Jensen, 2017), as well as its intense carbon sequestration potential. In particular, DIC was supplied at a much higher rate from the seagrass zone to the coral zone than from the mangrove zone to the seagrass zone (Fig. 5). This high supply to the coral zone might be due to the inflow of DIC from the mangrove zone and the further addition of DIC to the seagrass zone by OM degradation (Fig. 4).

The present study showed that about one-third of the sedimentary OM in the seagrass zone consisted of terrestrial OM (Table 3). This result is in agreement with previous studies reporting efficient storage of mangrove-derived OM in seagrass sediments (Bouillon et al., 2007; Walton et al., 2014; Chen et al., 2017). The contribution of terrestrial OM to sedimentary OM was much higher than its contribution to the POM pool, suggesting that selective burial of terrestrial OM was more efficient than burial of oceanic OM (Table 3; Watanabe and Kuwae, 2015).

Aromatic and refractory CDOM decreased as salinity increased towards seagrass and coral waters (Fig. 3i and j). This result indicates that mangrove-derived DOM was composed mostly of recalcitrant, higher molecular weight polymeric structures, whereas seagrass-derived DOM included relatively high concentrations of easily degradable proteinaceous components (Scully et al., 2004).

Contrary to the majority of other global observations, in the present study the seagrass surrounding waters acted as a net source of CO_2. Seagrass meadows often show net autotrophic activity with high carbon sequestration potential (Duarte et al., 2010; Watanabe and Kuwae, 2015; Olivé et al., 2016; Ganguly et al., 2017), so that on a millennial time scale they act as a net CO_2 sink (Tokoro et al., 2014) and store carbon (Kennedy et al., 2010; Fourqurean et al., 2012; Greiner et al., 2013). The most plausible reason for seagrass to act as a net CO_2 source is the addition of allochthonous carbon forms from upstream, with both riverine freshwater and mangrove-derived inputs (Tokoro et al., 2014; Bouillon et al., 2007; Macklin et al., 2019). In the present study, the input of allochthonous DIC and high pCO_2 water as well as the degradation of both allochthonous and autochthonous OM together played crucial roles in making the seagrass zone a CO_2 source (Figs. 4 and 5). However, the DIC uptake capacity of the seagrass zone substantially reduced pCO_2(water) in the seagrass zone compared to that in the mangrove zone (Table 1, Fig. 2).

4.3. The role of the coral zone in the continuum system

The mass-balance model (Fig. 5) shows that the coral zone acted as a net sink of DOC, although in general coral ecosystems act as a net source of POC and DOC (Tanaka et al., 2009; Naumann et al., 2010; Nakajima et al., 2010; Haas et al., 2011). Furthermore, the DOC and CDOM results indicate that DOM was removed from the coral zone (Figs. 3 and 5). Removal of DOC from the water column through photochemical and microbial degradation would offset autochthonous DOM production and imports from upstream (Zepp et al., 2008; Andersson and Mackenzie, 2012; Mostofa et al., 2016). Because the study site is a shallow coast (mean depth ~1.12 m), sunlight reaches the bottom and would efficiently degrade DOM. Furthermore, the relatively high water temperature in the coral zone would facilitate microbial degradation (Table 1). Nelson et al. (2011) also reported a coral reef ecosystem acting as a net sink of DOC and suggested that the depletion of DOC could be attributed to decomposition of DOM by bacterioplankton (Tanaka et al., 2011a, 2011b). Further study of microbial abundance and community composition has the potential to elucidate the OM degradation pathway and DOC removal in coral reef ecosystems.

The coral zone in the present study acted as a weak source of atmospheric CO_2 and showed higher uptakes of TAlk and DIC than the other zones (Figs. 3 and 5), in addition to a stronger negative correlation between pCO_2(water) and DO saturation (Fig. S4, Supplementary material). Coral-adjacent waters (mainly coral-dominated reef systems) have been reported to be mostly a net source of CO_2 (Ware et al., 1991; Gattuso et al., 1993; Frankignoulle et al., 1996; Gattuso et al., 1999; Kawahata et al., 2000); however, coral reef systems can act as a net sink for CO_2 when photosynthetic activity exceeds calcification (Kayanne et al., 1995) because of the high abundance of macroalgae and other symbiotic algae (Yamamuro and Kayanne, 1995; Kraines et al., 1997). In the present study, the coral zone acted as a sink for

TAlk and DIC and as a weak net source of CO_2. The strong negative relationship between pCO_2(water) and O_2 saturation in the coral zone indicates that biological uptake and metabolism play a crucial role in pCO_2 (water) dynamics in the coral water (Fig. S4, Supplementary material; Yan et al., 2016). Even though the chlorophyll-*a* concentration was low in the coral zone (Table 1), primary production by phytoplankton would contribute to the community metabolism. The net balance between calcification and organic carbon production in a coral reef ecosystem can determine whether it is a source or sink of atmospheric CO_2 (Bates, 2002). The combination of negative ΔDIC with negative $\Delta\delta^{13}C_{DIC}$ in some samples from the coral zone (Fig. 4) is a result of carbonate precipitation. In contrast, the combination of negative ΔDIC with positive $\Delta\delta^{13}C_{DIC}$, an indicator of primary productivity or CO_2 outgassing, was not observed, which indicates that calcification predominates over organic carbon production in this coral zone (Yan et al., 2016). We further argue that the character of the zone as a CO_2 source can be attributed to the allochthonous carbon supply, as Kawahata et al. (2000) observed in a nearby fringing reef, along with net calcification in the coral zone.

4.4. Uncertainty of the lateral carbon flux and air–water CO_2 flux estimation

In the present study, the lateral carbon flux was estimated under the assumption that water exchanges occurred precisely between the constructed boxes (Fig. S2, Supplementary material); as a result, there is possible uncertainty in the lateral flux estimation. We constructed the boxes according to the ecosystem connectivity among the three ecosystems described by Aliño and Muallil (2014), who assumed that such closely spaced ecosystems would necessarily be interconnected. The main reason for positioning the hypothetical boxes as shown in Fig. S2 (Supplementary material) was to take into account the longitudinal connectivity from the mouth of the Yutsun River and the surrounding mangrove ecosystem through the seagrass beds and the coral ecosystem. We believe that if we were to construct similar series of hypothetical boxes parallel to and on either side of the present boxes, they would also represent the same ecosystem continuum. The angle of alignment of the constructed boxes with respect to the shoreline was selected to accord with the measured direction of wave propagation in the study area, which is mainly from the north-east (Masayuki Banno, Port and Airport Research Institute, Japan, personal communication). Hence, we believe that by orienting and placing the boxes in this way, we minimized the uncertainty of carbon flux estimation between the boxes.

Another possible source of uncertainty in the estimation of the air–water CO_2 flux and lateral carbon fluxes arises from the fact that sampling was carried out during only two diurnal cycles in each zone, with a corresponding absence of seasonal variability in the resulting dataset. However, characterizing the spring-to-neap variability along with the seasonal variability was not our main goal.

Comparing the carbon forms between water and sediment might include uncertainty, because carbon forms in the surface water vary on a short timescale (days) and are regulated by processes such as the advection pathway, residence time, and cycling of waters, whereas SOC accumulation varies on a much longer timescale (seasons or even years). We argue, however, that our comparison is valid because POC is the major form of the carbon deposited in the sediment in the study area, and the POC concentration has been observed to vary annually over a narrow range, for example, near Ishigaki Island, close to the present study area (Miyajima et al., 2007).

5. Conclusion

This study quantified lateral carbon fluxes and the air–water CO_2 flux in a subtropical mangrove-seagrass-coral continuum and their significance. Our findings suggest that lateral fluxes of carbon have significant effects on the CO_2 dynamics of vegetated coastal ecosystems. The lateral export of carbon, mainly in the form of DIC and DOC, from the terrestrial zone, including mangroves, had a negative effect on CO_2 uptake in the seagrass and coral zones. However, the coral zone received carbon from the seagrass zone and acted as a net sink for TAlk, DIC, and DOC, indicating that high biological metabolic activity in this zone offset the effect of the allochthonous carbon load. Overall, the continuum ecosystem acted as a net sink for TAlk and DIC as well as a net source for DOC, POC, and atmospheric CO_2. We showed that the air–water CO_2 flux in the continuum ecosystem was affected by the metabolism in each habitat and by exchanges of inorganic and organic carbon. Future studies should assess the interactive effects of other ecosystem features such as hydrological energy, nutrient and sediment loads, and food webs, on CO_2 sequestration in the continuum. Further spatial and temporal upscaling and comparison of both lateral carbon fluxes and the air–water CO_2 flux among these three important coastal ecosystems and discussion of their significance to CO_2 dynamics should improve estimates of the global carbon budget.

CRediT authorship contribution statement

Anirban Akhand: Conceptualization, Methodology - field work, sample and data analyses, Writing - original draft preparation, reviewing and editing.
Kenta Watanabe: Conceptualization, Methodology - field work, sample and data analyses, Writing - original draft preparation, reviewing and editing.
Abhra Chanda: Methodology - field work, sample and data analyses, Writing - reviewing and editing.
Tatsuki Tokoro: Methodology - field work, sample and data analyses, Writing - reviewing and editing.
Kunal Chakraborty: Methodology - data analyses, Modelling, Writing - reviewing and editing.
Hirotada Moki: Methodology - sample and data analyses, Writing - reviewing and editing.
Toko Tanaya: Methodology - sample and data analyses, Writing - reviewing and editing.
Jayashree Ghosh: Methodology - modelling, Writing - reviewing and editing.
Tomohiro Kuwae: Conceptualization, Supervision, Writing - reviewing and editing.

Declaration of competing interest

The authors declare that they have no known competing financial interests or personal relationships that could have appeared to influence the work reported in this paper.

Acknowledgements

We are grateful for funding provided by the Environmental Research and Technology Development Fund (S-14) and the Japan Society for the Promotion of Science (KAKENHI grants 18H04156 and 19K20500). We are indebted to Ms. N. Umegaki for help with the chemical analyses.

Appendix A. Supplementary material

Supplementary material to this article can be found online at https://doi.org/10.1016/j.scitotenv.2020.142190.

References

Agata, S., 2006. Characteristics of hydrogen and oxygen isotopic compositions and chemistry of precipitation on Ishigaki Island in Okinawa, Japan. Chikyukagaku 40, 111–123.
Aliño, P., Muallil, R., 2014. The need for institutional networking in integrated coastal management: interconnectivity among coral reefs, seagrass beds and mangroves. Mangrove Proceedings. vol. 7, pp. 66–72 indd.

Andersson, A.J., Mackenzie, F.T., 2012. Revisiting four scientific debates in ocean acidification research. Biogeosciences 9 (3), 893–905. https://doi.org/10.5194/bg-9-893-2012.

Bates, N.R., 2002. Seasonal variability of the effect of coral reefs on seawater CO_2 and air - sea CO_2 exchange. Limnol. Oceanogr. 47 (1), 43–52. https://doi.org/10.4319/lo.2002.47.1.0043.

Bergamaschi, B.A., Krabbenhoft, D.P., Aiken, G.R., Patino, E., Rumbold, D.G., Orem, W.H., 2012. Tidally driven export of dissolved organic carbon, total mercury, and methylmercury from a mangrove-dominated estuary. Environ. Sci. Technol. 46 (3), 1371–1378. https://doi.org/10.1021/es2029137.

Borges, A., Abril, G., 2011. Carbon dioxide and methane dynamics in estuaries. In: McLusky, D., Wolansky, E. (Eds.), Treatise on Estuarine and Coastal Science. Biogeochemistry vol. 5. Academic Press, USA, pp. 119–161.

Borges, A.V., Vanderborght, J.P., Schiettecatte, L.S., Gazeau, F., Ferrón-Smith, S., Delille, B., Frankignoulle, M., 2004. Variability of the gas transfer velocity of CO_2 in a macrotidal estuary (the Scheldt). Estuaries 27 (4), 593–603. https://doi.org/10.1007/BF02907647.

Borges, A.V., Delille, B., Frankignoulle, M., 2005. Budgeting sinks and sources of CO_2 in the coastal ocean: diversity of ecosystems counts. Geophys. Res. Lett. 32 (14), L14601. https://doi.org/10.1029/2005GL023053.

Borges, A., Abril, G., Bouillon, S., 2018. Carbon dynamics and CO_2 and CH_4 outgassing in the Mekong delta. Biogeosciences 15, 1093–1114. https://doi.org/10.5194/bg-15-1093-2018.

Bouillon, S., Boschker, H.T.S., 2006. Bacterial carbon sources in coastal sediments: a cross-system analysis based on stable isotope data of biomarkers. Biogeosciences 3 (2), 175–185. https://doi.org/10.5194/bg-3-175-2006.

Bouillon, S., Middelburg, J.J., Dehairs, F., Borges, A.V., Abril, G., Flindt, M.R., Ulomi, S., Kristensen, E., 2007. Importance of intertidal sediment processes and porewater exchange on the water column biogeochemistry in a pristine mangrove creek (Ras Dege, Tanzania). Biogeosciences. 4, 311–322. https://doi.org/10.5194/bg-4-311-2007.

Bouillon, S., Borges, A.V., Castañeda-Moya, E., Diele, K., Dittmar, T., Duke, N.C., Kristensen, E., Lee, S.Y., Marchand, C., Middelburg, J.J., Rivera-Monroy, V.H., 2008. Mangrove production and carbon sinks: a revision of global budget estimates. Glob. Biogeochem. Cycles 22 (2), GB2013. https://doi.org/10.1029/2007GB003052.

Boyd, M.J., Pilgrim, D.H., Cordery, I., 1979. A storage routing model based on catchment geomorphology. J. Hydrol. 42 (3–4), 209–230. https://doi.org/10.1016/0022-1694(79)90048-9.

Brandano, M., Cuffaro, M., Gaglianone, G., Petricca, P., Stagno, V., Mateu-Vicens, G., 2016. Evaluating the role of seagrass in Cenozoic CO_2 variations. Front. Environ. Sci. 4, 72. https://doi.org/10.3389/fenvs.2016.00072.

Call, M., Santos, I.R., Dittmar, T., de Rezende, C.E., Asp, N.E., Maher, D.T., 2019. High porewater derived CO_2 and CH_4 emissions from a macro-tidal mangrove creek in the Amazon region. Geochim. Cosmochim. Acta 247, 106–120. https://doi.org/10.1016/j.gca.2018.12.029.

Camp, E.F., Suggett, D.J., Gendron, G., Jompa, J., Manfrino, C., Smith, D.J., 2016. Mangrove and seagrass beds provide different biogeochemical services for corals threatened by climate change. Front. Mar. Sci. 3, 52. https://doi.org/10.3389/fmars.2016.00052.

Chen, G., Azkab, M.H., Chmura, G.L., Chen, S., Sastrosuwondo, P., Ma, Z., Dharmawan, I.W.E., Yin, X., Chen, B., 2017. Mangroves as a major source of soil carbon storage in adjacent seagrass meadows. Sci. Rep. 7, 42406. https://doi.org/10.1038/srep42406.

David, F., Meziane, T., Tran-Thi, N.T., Van, V.T., Thanh-Nho, N., Taillardat, P., Marchand, C., 2018. Carbon biogeochemistry and CO_2 emissions in a human impacted and mangrove dominated tropical estuary (Can Gio, Vietnam). Biogeochemistry 138 (3), 261–275. https://doi.org/10.1007/s10533-018-0444-z.

De Madron, X.D., Denis, L., Diaz, F., Garcia, N., Guieu, C., Grenz, C., Loÿe-Pilot, M.D., Ludwig, W., Moutin, T., Raimbault, P., Ridame, C., 2003. Nutrients and carbon budgets for the Gulf of Lion during the Moogli cruises. Oceanol. Acta 26 (4), 421–433. https://doi.org/10.1016/S0399-1784(03)00024-0.

Dickson, A.G., Sabine, C.L., Christian, J.R., 2007. Guide to Best Practices for Ocean CO_2 Measurements. PICES Special Publication, North Pacific Marine Science Organization, Canada.

Duarte, C.M., Cebrián, J., 1996. The fate of marine autotrophic production. Limnol. Oceanogr. 41 (8), 1758–1766. https://doi.org/10.4319/lo.1996.41.8.1758.

Duarte, C.M., Krause-Jensen, D., 2017. Export from seagrass meadows contributes to marine carbon sequestration. Front. Mar. Sci. 4, 13. https://doi.org/10.3389/fmars.2017.00013.

Duarte, C.M., Marbà, N., Gacia, E., Fourqurean, J.W., Beggins, J., Barrón, C., Apostolaki, E.T., 2010. Seagrass community metabolism: assessing the carbon sink capacity of seagrass meadows. Glob. Biogeochem. Cycle. 24 (4). https://doi.org/10.1029/2010GB003793.

Fichot, C.G., Benner, R., 2012. The spectral slope coefficient of chromophoric dissolved organic matter (S275–295) as a tracer of terrigenous dissolved organic carbon in river-influenced ocean margins. Limnol. Oceanogr. 57 (5), 1453–1466. https://doi.org/10.4319/lo.2012.57.5.1453.

Fourqurean, J.W., Duarte, C.M., Kennedy, H., Marbà, N., Holmer, M., Mateo, M.A., Apostolaki, E.T., Kendrick, G.A., Krause-Jensen, D., McGlathery, K.J., Serrano, O., 2012. Seagrass ecosystems as a globally significant carbon stock. Nat. Geosci. 5 (7), 505–509. https://doi.org/10.1038/ngeo1477.

Frankignoulle, M., Gattuso, J.P., Biondo, R., Bourge, I., Copin-Montégut, G., Pichon, M., 1996. Carbon fluxes in coral reefs. II. Eulerian study of inorganic carbon dynamics and measurement of air-sea CO_2 exchanges. Mar. Ecol. Prog. Ser. 145, 123–132. https://doi.org/10.3354/meps145123.

Fry, B., 2006. Stable Isotope Ecology. vol. 521. Springer, New York.

Ganguly, D., Singh, G., Ramachandran, P., Selvam, A.P., Banerjee, K., Ramachandran, R., 2017. Seagrass metabolism and carbon dynamics in a tropical coastal embayment. Ambio 46 (6), 667–679. https://doi.org/10.1007/s13280-017-0916-8.

Gattuso, J.P., Pichon, M., Delesalle, B., Frankignoulle, M., 1993. Community metabolism and air-sea CO_2 fluxes in a coral reef ecosystem (Moorea, French Polynesia). Mar. Ecol. Prog. Ser. 96 (3), 259–267. https://www.jstor.org/stable/24833554.

Gattuso, J.P., Allemand, D., Frankignoulle, M., 1999. Photosynthesis and calcification at cellular, organismal and community levels in coral reefs: a review on interactions and control by carbonate chemistry. Am. Zool. 39 (1), 160–183. https://doi.org/10.1093/icb/39.1.160.

Gillis, L.G., Ziegler, A.D., van Oevelen, D., Cathalot, C., Herman, P.M., Wolters, J.W., Bouma, T.J., 2014. Tiny is mighty: seagrass beds have a large role in the export of organic material in the tropical coastal zone. PLoS One 9 (11), e111847. https://doi.org/10.1371/journal.pone.0111847.

Gleeson, J., Santos, I.R., Maher, D.T., Golsby-Smith, L., 2013. Groundwater–surface water exchange in a mangrove tidal creek: evidence from natural geochemical tracers and implications for nutrient budgets. Mar. Chem. 156, 27–37. https://doi.org/10.1016/j.marchem.2013.02.001.

Gnanamoorthy, P., Selvam, V., Burman, P.K.D., Chakraborty, S., Karipot, A., Nagarajan, R., Ramasubramanian, R., Song, Q., Zhang, Y., Grace, J., 2020. Seasonal variations of net ecosystem (CO_2) exchange in the Indian tropical mangrove forest of Pichavaram. Estuarine, Coast. Shelf Sci., 106828 https://doi.org/10.1016/j.ecss.2020.106828.

Gordon, D.C., Boudreau, P.R., Mann, K.H., Ong, J.E., Silvert, W.L., Smith, S.V., Wattayakorn, G., Wulff, F., Yanagi, T., 1996. LOICZ Biogeochemical Modelling Guidelines (Vol. 5), Yerseke: LOICZ Core Project. Netherlands Institute for Sea Research, Netherland.

Greiner, J.T., McGlathery, K.J., Gunnell, J., McKee, B.A., 2013. Seagrass restoration enhances "blue carbon" sequestration in coastal waters. PLoS One 8 (8). https://doi.org/10.1371/journal.pone.0072469.

Gulliver, A., Carnell, P.E., Trevathan-Tackett, S.M., Duarte de Paula Costa, M., Masqué, P., Macreadie, P.I., 2020. Estimating the potential blue carbon gains from tidal marsh rehabilitation: a case study from south eastern Australia. Front. Mar. Sci. 7, 403. https://doi.org/10.3389/fmars.2020.00403.

Haas, A.F., Nelson, C.E., Kelly, L.W., Carlson, C.A., Rohwer, F., Leichter, J.J., Wyatt, A., Smith, J.E., 2011. Effects of coral reef benthic primary producers on dissolved organic carbon and microbial activity. PLoS One 6 (11), e27973. https://doi.org/10.1371/journal.pone.0027973.

Harborne, A.R., Mumby, P.J., Micheli, F., Perry, C.T., Dahlgren, C.P., Holmes, K.E., Brumbaugh, D.R., 2006. The functional value of Caribbean coral reef, seagrass and mangrove habitats to ecosystem processes. Adv. Mar. Biol. 50, 57–189. https://doi.org/10.1016/S0065-2881(05)50002-6.

Heck, K.L., Carruthers, T.J., Duarte, C.M., Hughes, A.R., Kendrick, G., Orth, R.J., Williams, S.W., 2008. Trophic transfers from seagrass meadows subsidize diverse marine and terrestrial consumers. Ecosystems 11 (7), 1198–1210. https://doi.org/10.1007/s10021-008-9155-y.

Hemminga, M.A., Slim, F., Kazungu, J., Ganssen, G.M., Nieuwenhuize, J., Kruyt, N.M., 1994. Carbon outwelling from a mangrove forest with adjacent seagrass beds and coral reefs (Gazi Bay, Kenya). Mar. Ecol. Prog. Ser. 106.

Huxham, M., Whitlock, D., Githaiga, M., Dencer-Brown, A., 2018. Carbon in the coastal seascape: how interactions between mangrove forests, seagrass meadows and tidal marshes influence carbon storage. Current forestry reports 4 (2), 101–110. https://doi.org/10.1007/s40725-018-0077-4.

Jähne, B., Heinz, G., Dietrich, W., 1987. Measurement of the diffusion coefficients of sparingly soluble gases in water. J. Geophys. Res.: Oceans. 92 (C10), 10767–10776. https://doi.org/10.1029/JC092iC10p10767.

Kao, S.J., Liu, K.K., 2000. Stable carbon and nitrogen isotope systematics in a human-disturbed watershed (Lanyang-Hsi) in Taiwan and the estimation of biogenic particulate organic carbon and nitrogen fluxes. Glob. Biogeochem. Cycles 14 (1), 189–198. https://doi.org/10.1029/1999GB900079.

Kawahata, H., Yukino, I., Suzuki, A., 2000. Terrestrial influences on the Shiraho fringing reef, Ishigaki Island, Japan: high carbon input relative to phosphate. Coral Reefs 19 (2), 172–178. https://doi.org/10.1007/s003380000093.

Kayanne, H., Suzuki, A., Saito, H., 1995. Diurnal changes in the partial pressure of carbon dioxide in coral reef water. Science 269 (5221). https://doi.org/10.1126/science.269.5221.214.

Kayanne, H., Hata, H., Kudo, S., Yamano, H., Watanabe, A., Ikeda, Y., Nozaki, K., Kato, K., Negishi, A., Saito, H., 2005. Seasonal and bleaching-induced changes in coral reef metabolism and CO_2 flux. Glob. Biogeochem. Cycles 19 (3), GB3015. https://doi.org/10.1029/2004GB002400.

Kennedy, H., Beggins, J., Duarte, C.M., Fourqurean, J.W., Holmer, M., Marbà, N., Middelburg, J.J., 2010. Seagrass sediments as a global carbon sink: isotopic constraints. Glob. Biogeochem. Cycles 24 (4). https://doi.org/10.1029/2010GB003848.

Kimura, T., 1975. The Storage Function Model, Tokyo Publishing Company Kawanabe, (in Japanese) (Japan).

Kondo, J., 2000. Atmospheric Science Near the Ground Surface. University of Tokyo, Japan.

Koshiba, S., Besebes, M., Soaladaob, K., Isechal, A.L., Victor, S., Golbuu, Y., 2013. Palau's taro fields and mangroves protect the coral reefs by trapping eroded fine sediment. Wetl. Ecol. Manag. 21 (3), 157–164. https://doi.org/10.1007/s11273-013-9288-4.

Kraines, S., Suzuki, Y., Omori, T., Shitashima, K., Kanahara, S., Komiyama, H., 1997. Carbonate dynamics of the coral reef system at Bora Bay, Miyako Island. Mar. Ecol. Prog. Ser. 156, 1–16. https://doi.org/10.3354/meps156001.

Krüger, J.P., Leifeld, J., Glatzel, S., Szidat, S., Alewell, C., 2015. Biogeochemical indicators of peatland degradation-a case study of a temperate bog in northern Germany. Biogeosciences 12, 2861–2871. https://doi.org/10.5194/bg-12-2861-2015.

Kuwae, T., Hori, M., 2019. The future of blue carbon: addressing global environmental issues. In: Kuwae, T., Hori, M. (Eds.), Blue Carbon in Shallow Coastal Ecosystems. Springer, Singapore, pp. 347–373.

Kuwae, T., Beninger, P.G., Decottignies, P., Mathot, K.J., Lund, D.R., Elner, R.W., 2008. Biofilm grazing in a higher vertebrate: the western sandpiper, Calidris mauri. Ecology 89 (3), 599–606. https://doi.org/10.1890/07-1442.1.

Langodan, S., Antony, C., Shanas, P.R., Dasari, H.P., Abualnaja, Y., Knio, O., Hoteit, I., 2020. Wave modeling of a reef-sheltered coastal zone in the Red Sea. Ocean Eng. 207, 107378. https://doi.org/10.1016/j.oceaneng.2020.107378.

Liss, P.S., Merlivat, L., 1986. Air-sea gas exchange rates: introduction and synthesis. In: Buat-Ménard, P. (Ed.), The Role of Air-Sea Exchange in Geochemical Cycling. Springer, Dordrecht, pp. 113–127.

Lønborg, C., Calleja, M.L., Fabricius, K.E., Smith, J.N., Achterberg, E.P., 2019. The Great Barrier Reef: a source of CO_2 to the atmosphere. Mar. Chem. 210, 24–33. https://doi.org/10.1016/j.marchem.2019.02.003.

Loneragan, N.R., Bunn, S.E., Kellaway, D.M., 1997. Are mangroves and seagrasses sources of organic carbon for penaeid prawns in a tropical Australian estuary? A multiple stable-isotope study. Mar. Biol. 130 (2), 289–300. https://doi.org/10.1007/s002270050248.

Lorenzen, C.J., 1967. Determination of chlorophyll and pheo-pigments: spectrophotometric equations 1. Limnol. Oceanogr. 12 (2), 343–346. https://doi.org/10.4319/lo.1967.12.2.0343.

Lovelock, C.E., Duarte, C.M., 2019. Dimensions of Blue Carbon and emerging perspectives. Biol. Lett. 15 (3), 20180781. https://doi.org/10.1098/rsbl.2018.0781.

Macklin, P.A., Suryaputra, I.G.N.A., Maher, D.T., Murdiyarso, D., Santos, I.R., 2019. Drivers of CO_2 along a mangrove-seagrass transect in a tropical bay: delayed groundwater seepage and seagrass uptake. Cont. Shelf Res. 172, 57–67. https://doi.org/10.1016/j.csr.2018.10.008.

Macreadie, P.I., Nielsen, D.A., Kelleway, J.J., Atwood, T.B., Seymour, J.R., Petrou, K., Connolly, R.M., Thomson, A.C.G., Trevathan-Tackett, S.M., Ralph, P.J., 2017. Can we manage coastal ecosystems to sequester more blue carbon? Front. Ecol. Environ. 15 (4), 206–213. https://doi.org/10.1002/fee.1484.

Macreadie, P.I., Anton, A., Raven, J.A., Beaumont, N., Connolly, R.M., Friess, D.A., Kelleway, J.J., Kennedy, H., Kuwae, T., Lavery, P.S., Lovelock, C.E., et al., 2019. The future of Blue Carbon science. Nat. Commun. 10 (1), 1–13. https://doi.org/10.1038/s41467-019-11693-w.

Maher, D.T., Santos, I.R., Golsby-Smith, L., Gleeson, J., Eyre, B.D., 2013. Groundwater-derived dissolved inorganic and organic carbon exports from a mangrove tidal creek: the missing mangrove carbon sink? Limnol. Oceanogr. 58 (2), 475–488. https://doi.org/10.4319/lo.2013.58.2.0475.

Maher, D.T., Call, M., Santos, I.R., Sanders, C.J., 2018. Beyond burial: lateral exchange is a significant atmospheric carbon sink in mangrove forests. Biol. Lett. 14 (7), 20180200. https://doi.org/10.1098/rsbl.2018.0200.

Martins, K.A., Pereira, P.D.S., Esteves, L.S., Williams, J., 2019. The role of coral reefs in coastal protection: analysis of beach morphology. J. Coast. Res. 92 (SI), 157–164. https://doi.org/10.2112/SI92-018.1.

Mazda, Y., Ikeda, Y., 2006. Behavior of the groundwater in a riverine-type mangrove forest. Wetl. Ecol. Manag. 14 (6), 477–488. https://doi.org/10.4319/lo.2013.58.2.0475.

Mcleod, E., Chmura, G.L., Bouillon, S., Salm, R., Björk, M., Duarte, C.M., Lovelock, C.E., Schlesinger, W.H., Silliman, B.R., 2011. A blueprint for blue carbon: toward an improved understanding of the role of vegetated coastal habitats in sequestering CO_2. Front. Ecol. Environ. 9, 552–560. https://doi.org/10.1890/110004.

Miyajima, T., Miyajima, Y., Hanba, Y.T., Yoshii, K., Koitabashi, T., Wada, E., 1995. Determining the stable isotope ratio of total dissolved inorganic carbon in lake water by GC/C/IIRMS. Limnol. Oceanogr. 40 (5), 994–1000. https://doi.org/10.4319/lo.1995.40.5.0994.

Miyajima, T., Hata, H., Umezawa, Y., Kayanne, H., Koike, I., 2007. Distribution and partitioning of nitrogen and phosphorus in a fringing reef lagoon of Ishigaki Island, northwestern Pacific. Mar. Ecol. Prog. Ser. 341, 45–57. https://doi.org/10.3354/meps341045.

Mook, W.G., Tan, F.C., 1991. Stable carbon isotopes in rivers and estuaries. Biogeochemistry of Major World Rivers, SCOPE. vol. 42. John Wiley, UK, pp. 245–264.

Mostofa, K.M., Liu, C.Q., Zhai, W., Minella, M., Vione, D.V., Gao, K., Minakata, D., Arakaki, T., Yoshioka, T., Hayakawa, K., Konohira, E., 2016. Reviews and syntheses: ocean acidification and its potential impacts on marine ecosystems. Biogeosciences 13, 1767–1787. https://doi.org/10.5194/bg-13-1767-2016.

Nakajima, R., Yoshida, T., Fujita, K., Nakayama, A., Fuchinoue, Y., Othman, B.H.R., Toda, T., 2010. Release of particulate and dissolved organic carbon by the scleractinian coral *Acropora formosa*. Bull. Mar. Sci. 86 (4), 861–870. https://doi.org/10.5343/bms.2009.1069.

Naumann, M.S., Haas, A., Struck, U., Mayr, C., el-Zibdah, M., Wild, C., 2010. Organic matter release by dominant hermatypic corals of the Northern Red Sea. Coral Reefs 29 (3), 649–659. https://doi.org/10.1007/s00338-010-0612-7.

Nelson, C.E., Alldredge, A.L., McCliment, E.A., Amaral-Zettler, L.A., Carlson, C.A., 2011. Depleted dissolved organic carbon and distinct bacterial communities in the water column of a rapid-flushing coral reef ecosystem. The ISME Journal 5 (8), 1374–1387. https://doi.org/10.1038/ismej.2011.12.

O'Connor, J.J., Fest, B.J., Sievers, M., Swearer, S.E., 2020. Impacts of land management practices on blue carbon stocks and greenhouse gas fluxes in coastal ecosystems—a meta-analysis. Glob. Chang. Biol. 26 (3), 1354–1366. https://doi.org/10.1111/gcb.14946.

Odum, W.E., Heald, E.J., 1975. Mangrove forests and aquatic productivity. In: Hasler, A.D. (Ed.), Coupling of Land and Water Systems. Springer, Berlin, Heidelberg, pp. 129–136.

Olivé, I., Silva, J., Costa, M.M., Santos, R., 2016. Estimating seagrass community metabolism using benthic chambers: the effect of incubation time. Estuar. Coast. 39 (1), 138–144. https://doi.org/10.1007/s12237-015-9973-z.

Otani, S., Endo, T., 2019. CO_2 flux in tidal flats and salt marshes. In: Kuwae, T., Hori, M. (Eds.), Blue Carbon in Shallow Coastal Ecosystems. Springer, Singapore, pp. 223–250.

Parnell, A.C., Inger, R., Bearhop, S., Jackson, A.L., 2010. Source partitioning using stable isotopes: coping with too much variation. PLoS One 5 (3). https://doi.org/10.1371/journal.pone.0009672.

Pendleton, L., Donato, D.C., Murray, B.C., Crooks, S., Jenkins, W.A., Sifleet, S., Craft, C., Fourqurean, J.W., Kauffman, J.B., Marbà, N., Megonigal, P., 2012. Estimating global "blue carbon" emissions from conversion and degradation of vegetated coastal ecosystems. PLoS One 7 (9), e43542. https://doi.org/10.1371/journal.pone.0043542.

Perdue, E.M., Koprivnjak, J.F., 2007. Using the C/N ratio to estimate terrigenous inputs of organic matter to aquatic environments. Estuar. Coast. Shelf Sci. 73 (1–2), 65–72. https://doi.org/10.1016/j.ecss.2006.12.021.

Ray, R., Weigt, M., 2018. Seasonal and habitat-wise variations of creek water particulate and dissolved organic carbon in arid mangrove (the Persian Gulf). Cont. Shelf Res. 165, 60–70. https://doi.org/10.1016/j.csr.2018.06.009.

Raymond, P.A., Cole, J.J., 2001. Gas exchange in rivers and estuaries: choosing a gas transfer velocity. Estuaries 24 (2), 312–317. https://doi.org/10.2307/1352954.

Rogers, C.S., 2017. A unique coral community in the mangroves of Hurricane Hole, St. John, US Virgin Islands. Diversity 9 (3), 29. https://doi.org/10.3390/d9030029.

Rosentreter, J.A., Maher, D.T., Erler, D.V., Murray, R., Eyre, B.D., 2018. Seasonal and temporal CO_2 dynamics in three tropical mangrove creeks–a revision of global mangrove CO_2 emissions. Geochim. Cosmochim. Acta 222, 729–745. https://doi.org/10.1016/j.gca.2017.11.026.

Roth, F., Karcher, D.B., Rädecker, N., Hohn, S., Carvalho, S., Thomson, T., Saalmann, F., Voolstra, C.R., Kűrten, B., Struck, U., Jones, B.H., Wild, C., 2020. High rates of carbon and dinitrogen fixation suggest a critical role of benthic pioneer communities in the energy and nutrient dynamics of coral reefs. Funct. Ecol. https://doi.org/10.1111/1365-2435.13625.

Saito, H., Tamura, N., Kitano, H., Mito, A., Takahashi, C., Suzuki, A., Kayanne, H., 1995. A compact seawater pCO_2 measurement system with membrane equilibrator and non-dispersive infrared gas analyzer. Deep Sea Res. Part I: Oceanogr. Res. Pap. 42, 11–12. https://doi.org/10.1016/0967-0637(95)00090-9.

Santos, I.R., Eyre, B.D., Huettel, M., 2012. The driving forces of porewater and groundwater flow in permeable coastal sediments: a review. Estuar. Coast. Shelf Sci. 98, 1–15. https://doi.org/10.1016/j.ecss.2011.10.024.

Scully, N.M., Maie, N., Dailey, S.K., Boyer, J.N., Jones, R.D., Jaffé, R., 2004. Early diagenesis of plant-derived dissolved organic matter along a wetland, mangrove, estuary ecotone. Limnol. Oceanogr. 49 (5), 1667–1678. https://doi.org/10.4319/lo.2004.49.5.1667.

Sippo, J.Z., Maher, D.T., Tait, D.R., Holloway, C., Santos, I.R., 2016. Are mangroves drivers or buffers of coastal acidification? Insights from alkalinity and dissolved inorganic carbon export estimates across a latitudinal transect. Glob. Biogeochem. Cycle. 30 (5), 753–766. https://doi.org/10.1002/2015GB005324.

Su, Z., Qiu, G., Fan, H., Li, M., Fang, C., 2020. Changes in carbon storage and macrobenthic communities in a mangrove-seagrass ecosystem after the invasion of smooth cordgrass in southern China. Mar. Pollut. Bull. 152, 110887. https://doi.org/10.1016/j.marpolbul.2020.110887.

Tanaka, Y., Miyajima, T., Umezawa, Y., Hayashibara, T., Ogawa, H., Koike, I., 2009. Net release of dissolved organic matter by the scleractinian coral *Acropora pulchra*. J. Exp. Mar. Biol. Ecol. 377 (2), 101–106. https://doi.org/10.1016/j.jembe.2009.06.023.

Tanaka, Y., Ogawa, H., Miyajima, T., 2011a. Bacterial decomposition of coral mucus as evaluated by long-term and quantitative observation. Coral Reefs 30 (2), 443–449. https://doi.org/10.1007/s00338-011-0729-3.

Tanaka, Y., Ogawa, H., Miyajima, T., 2011b. Production and bacterial decomposition of dissolved organic matter in a fringing coral reef. J. Oceanogr. 67 (4), 427–437. https://doi.org/10.1007/s10872-011-0046-z.

Thornton, S.F., McManus, J., 1994. Application of organic carbon and nitrogen stable isotope and C/N ratios as source indicators of organic matter provenance in estuarine systems: evidence from the Tay Estuary, Scotland. Estuar. Coast. Shelf Sci. 38 (3), 219–233. https://doi.org/10.1006/ecss.1994.1015.

Tokoro, T., Hosokawa, S., Miyoshi, E., Tada, K., Watanabe, K., Montani, S., Kayanne, H., Kuwae, T., 2014. Net uptake of atmospheric CO_2 by coastal submerged aquatic vegetation. Glob. Chang. Biol. 20 (6), 1873–1884. https://doi.org/10.1111/gcb.12543.

Tomita, H., Hihara, T., Kako, S.I., Kubota, M., Kutsuwada, K., 2019. An introduction to J-OFURO3, a third-generation Japanese ocean flux data set using remote-sensing observations. J. Oceanogr. 75 (2), 171–194. https://doi.org/10.1007/s10872-018-0493-x.

Tremblay, L.B., Dittmar, T., Marshall, A.G., Cooper, W.J., Cooper, W.T., 2007. Molecular characterization of dissolved organic matter in a North Brazilian mangrove porewater and mangrove-fringed estuaries by ultrahigh resolution Fourier Transform-Ion Cyclotron Resonance mass spectrometry and excitation/emission spectroscopy. Mar. Chem. 105 (1–2), 15–29. https://doi.org/10.1016/j.marchem.2006.12.015.

Unsworth, R.K., Collier, C.J., Henderson, G.M., McKenzie, L.J., 2012. Tropical seagrass meadows modify seawater carbon chemistry: implications for coral reefs impacted by ocean acidification. Environment. Res. Lett. 7 (2), 024026. https://doi.org/10.1088/1748-9326/7/2/024026.

Victor, S., Golbuu, Y., Wolanski, E., Richmond, R.H., 2004. Fine sediment trapping in two mangrove-fringed estuaries exposed to contrasting land-use intensity, Palau, Micronesia. Wetl. Ecol. Manag. 12 (4), 277–283. https://doi.org/10.1007/s11273-005-8319-1.

Walton, M.E.M., Al-Maslamani, I., Skov, M.W., Al-Shaikh, I., Al-Ansari, I.S., Kennedy, H.A., Le Vay, L., 2014. Outwelling from arid mangrove systems is sustained by inwelling of seagrass productivity. Mar. Ecol. Prog. Ser. 507, 125–137. https://doi.org/10.3354/meps10827.

Wanninkhof, R., 1992. Relationship between wind speed and gas exchange over the ocean. J. Geophys. Res. Oceans 97 (C5), 7373–7382. https://doi.org/10.1029/92JC00188.

Ware, J.R., Smith, S.V., Reaka-Kudla, M.L., 1991. Coral reefs: sources or sinks of atmospheric CO_2? Coral Reefs 11 (3), 127–130. https://doi.org/10.1007/BF00255465.

Watanabe, K., Kuwae, T., 2015. How organic carbon derived from multiple sources contributes to carbon sequestration processes in a shallow coastal system? Glob. Chang. Biol. 21 (7), 2612–2623. https://doi.org/10.1111/gcb.12924.

Watanabe, A., Nakamura, T., 2019. Carbon dynamics in coral reefs. In: Kuwae, T., Hori, M. (Eds.), Blue Carbon in Shallow Coastal Ecosystems. Springer, Singapore, pp. 273–293.

Weiss, R., 1974. Carbon dioxide in water and seawater: the solubility of a non-ideal gas. Mar. Chem. 2 (3), 203–215. https://doi.org/10.1016/0304-4203(74)90015-2.

Wu, S.J., Ho, L.F., Yang, J.C., 2011. Application of modified nonlinear storage function on runoff estimation. J. Hydro-environ. Res. 5 (1), 37–47. https://doi.org/10.1016/j.jher.2010.09.003.

Xu, S., Yu, K., Fan, T., Jiang, W., Wang, R., Zhang, Y., Yue, Y., Wang, S., 2019. Coral reef carbonate δ13C records from the northern South China Sea: a useful proxy for seawater δ13C and the carbon cycle over the past 1.8 Ma. Glob. Planet. Chang. 182, 103003. https://doi.org/10.1016/j.gloplacha.2019.103003.

Yamamuro, M., Kayanne, H., 1995. Rapid direct determination of organic carbon and nitrogen in carbonate-bearing sediments with a Yanaco MT-5 CHN analyzer. Limnol. Oceanogr. 40 (5), 1001–1005. https://doi.org/10.4319/lo.1995.40.5.1001.

Yamano, H., Inoue, T., Adachi, H., Tsukaya, K., Adachi, R., Baba, S., 2019. Holocene sea-level change and evolution of a mixed coral reef and mangrove system at Iriomote Island, southwest Japan. Estuar. Coast. Shelf Sci. 220, 166–175. https://doi.org/10.1016/j.ecss.2019.03.001.

Yan, H., Yu, K., Shi, Q., Tan, Y., Liu, G., Zhao, M., Li, S., Chen, T., Wang, Y., 2016. Seasonal variations of seawater pCO2 and sea-air CO2 fluxes in a fringing coral reef, northern South China Sea. J. Geophys. Res.: Oceans 121 (1), 998–1008. https://doi.org/10.1002/2015JC011484.

Yates, K.K., Rogers, C.S., Herlan, J.J., Brooks, G.R., Smiley, N.A., Larson, R.A., 2014. Diverse coral communities in mangrove habitats suggest a novel refuge from climate change. Biogeosciences 4321. https://doi.org/10.5194/bg-11-4321-2014.

Zepp, R.G., Shank, G.C., Stabenau, E., Patterson, K.W., Cyterski, M., Fisher, W., Bartels, E., Anderson, S.L., 2008. Spatial and temporal variability of solar ultraviolet exposure of coral assemblages in the Florida Keys: importance of colored dissolved organic matter. Limnol. Oceanogr. 53 (5), 1909–1922. https://doi.org/10.4319/lo.2008.53.5.1909.